Arctic late Paleocene–early Eocene paleoenvironments with special emphasis on the Paleocene-Eocene thermal maximum (Lomonosov Ridge, Integrated Ocean Drilling Program Expedition 302)

Appy Sluijs,[1] Ursula Röhl,[2] Stefan Schouten,[3] Hans-J. Brumsack,[4] Francesca Sangiorgi,[1,3] Jaap S. Sinninghe Damsté,[3,5] and Henk Brinkhuis[1]

[1] We reconstruct the latest Paleocene and early Eocene (∼57–50 Ma) environmental trends in the Arctic Ocean and focus on the Paleocene-Eocene thermal maximum (PETM) (∼55 Ma), using strata recovered from the Lomonosov Ridge by the Integrated Ocean Drilling Program Expedition 302. The Lomonosov Ridge was still partially subaerial during the latest Paleocene and earliest Eocene and gradually subsided during the early Eocene. Organic dinoflagellate cyst (dinocyst) assemblages point to brackish and productive surface waters throughout the latest Paleocene and early Eocene. Dinocyst assemblages are cosmopolitan during this time interval, suggesting warm conditions, which is corroborated by TEX_{86}'-reconstructed temperatures of $15°–18°C$. Inorganic geochemistry generally reflects reducing conditions within the sediment and euxinic conditions during the upper lower Eocene. Spectral analysis reveals that the cyclicity, recorded in X-ray fluorescence scanning Fe data from close to Eocene thermal maximum 2 (∼53 Ma, presence confirmed by dinocyst stratigraphy), is related to precession. Within the lower part of the PETM, proxy records indicate enhanced weathering, runoff, anoxia, and productivity along with sea level rise. On the basis of total organic carbon content and variations in sediment accumulation rates, excess organic carbon burial in the Arctic Ocean appears to have contributed significantly to the sequestration of injected carbon during the PETM.

1. Introduction

[2] A wealth of biogeographical and geochemical evidence indicates that the late Paleocene to early Eocene (∼60–50 Ma) was the warmest interval of the Cenozoic [e.g., *Haq and Lohmann*, 1976; *Adams et al.*, 1990; *Hallock et al.*, 1991; *Zachos et al.*, 1994; *Bujak and Brinkhuis*, 1998; *Zachos et al.*, 2001; *Pearson et al.*, 2007]. During this time interval, both low- and high-latitude regions were much warmer than at present [*Zachos et al.*, 1993; *Fricke and Wing*, 2004; *Sluijs et al.*, 2006; *Pearson et al.*, 2007], which points to enhanced atmospheric concentrations of greenhouse gases being responsible for this global warmth [*Sloan and Rea*, 1996; *Huber et al.*, 2003; *Shellito et al.*,

2003; *Huber and Nof*, 2006]. Interest in this time interval is growing as a result of CO_2 proxy records indicating that CO_2 and associated feedbacks were, at least in part, responsible for this warmth, and that CO_2 concentrations were similar to those expected in the next centuries [*Pearson and Palmer*, 2000; *Demicco and Lowenstein*, 2003; *Yapp*, 2004; *Archer*, 2005; *Pagani et al.*, 2005; *Lowenstein and Demicco*, 2006].

[3] Superimposed on the late Paleocene and early Eocene broad warm interval, at least three episodes of rapid and marked warming occurred, termed the Paleocene-Eocene thermal maximum (PETM) (∼55 Ma), Eocene thermal maximum 2 (ETM2) (∼53 Ma) [*Lourens et al.*, 2005] and the informally named X event (∼52 Ma) [*Röhl et al.*, 2005]. Evidence for global warming during the PETM comes from the tetraether index of tetraether lipids consisting of 86 carbon atoms (TEX_{86}) sea surface temperature proxy [*Sluijs et al.*, 2006, 2007a; *Zachos et al.*, 2006], and methylation index of branched tetraethers (MBT) continental temperature proxy [*Weijers et al.*, 2007], oxygen isotope ($\delta^{18}O$) excursions in marine foraminiferal calcite [*Kennett and Stott*, 1991; *Thomas and Shackleton*, 1996; *Thomas et al.*, 2002; *Zachos et al.*, 2003, 2006] terrestrial carbonates [*Koch et al.*, 1995] and in phosphate of terrestrial skeletal apatite [*Fricke and Wing*, 2004], increased Mg/Ca values of planktonic and benthic foraminiferal calcite [*Zachos et al.*,

[1]Palaeoecology, Laboratory of Palaeobotany and Palynology, Institute of Environmental Biology, Utrecht University, Utrecht, Netherlands.
[2]Center for Marine Environmental Sciences, Bremen University, Bremen, Germany.
[3]Department of Marine Biogeochemistry and Toxicology, Royal Netherlands Institute for Sea Research, Den Burg, Texel, Netherlands.
[4]Institute for Chemistry and Biology of the Marine Environment, University of Oldenburg, Oldenburg, Germany.
[5]Department of Earth Sciences, Utrecht University, Utrecht, Netherlands.

2003; *Tripati and Elderfield*, 2005], poleward migrations of (sub)tropical marine plankton [*Kelly et al.*, 1996; *Crouch et al.*, 2001; *Hollis*, 2006; *Sluijs et al.*, 2007b] and terrestrial plant species [*Wing et al.*, 2005], and mammal migrations across high northern latitudes [*Bowen et al.*, 2002; *Smith et al.*, 2006]. The PETM is also characterized by the largest Cenozoic extinction of calcareous deep marine benthic foraminifera [*Thomas*, 1989; *Thomas and Shackleton*, 1996]. Associated with the PETM warming is a >2.5‰ negative carbon isotope ($\delta^{13}C$) excursion (CIE) measured on terrestrial and marine sedimentary carbon [*Kennett and Stott*, 1991; *Koch et al.*, 1992; *Thomas et al.*, 2002; *Pagani et al.*, 2006b]. The CIE is generally accepted to reflect a geologically rapid injection of ^{13}C-depleted carbon, in the form of CO_2 and/or CH_4, into the global exogenic carbon pool [*Dickens et al.*, 1995, 1997; *Higgins and Schrag*, 2006; *Pagani et al.*, 2006a; *Schouten et al.*, 2007b]. The rapid increase in CO_2 concentrations are also evidenced by severe deep marine carbonate dissolution [*Colosimo et al.*, 2005; *Zachos et al.*, 2005]. The recently discovered ETM2 [*Lourens et al.*, 2005] and X event [*Röhl et al.*, 2005] global warming episodes are also associated with negative carbon isotope excursions, deep see carbonate dissolution and biotic response. These CIEs are, however, smaller (∼2‰ and ∼1‰ for ETM2 and X, respectively) and also deep marine carbonate dissolution appears to have been less pronounced then during the PETM [*Lourens et al.*, 2005; *Röhl et al.*, 2005].

[4] While many low-latitude and midlatitude and limited high southern latitude PETM climate proxy records exist, northern high-latitude records are rare because of limited access to suitable core drilling sites. Information from this region, however, is vital to assess the status of global climate under high CO_2 concentrations because it defines end-members of important parameters, such as the meridional temperature gradient and atmospheric water transport. The few previous studies, from continental sections with generally poor dating, indicate that the Arctic Region was indeed warm during the latest Paleocene through early Eocene as indicated by floral [*Greenwood and Wing*, 1995], faunal [*Markwick*, 1998] and isotopic [*Bice et al.*, 1996; *Tripati et al.*, 2001] evidence. Recently, the first scientific drilling expedition was carried out in the Central Arctic Ocean (Integrated Ocean Drilling Program (IODP) Expedition 302, Arctic Coring Expedition (ACEX), Lomonosov Ridge). Initial ACEX results show that extremely high temperatures (between 17°C and 24°C) and low surface salinities prevailed in the Arctic around the PETM and during the early Eocene, while ventilation of the basin was sluggish [*Backman et al.*, 2006; *Brinkhuis et al.*, 2006; *Moran et al.*, 2006; *Pagani et al.*, 2006b; *Sluijs et al.*, 2006; L. M. Waddell and T. C. Moore, Salinity of the Eocene Arctic Ocean from oxygen isotope analysis of fish bone carbonate, submitted to *Paleoceanography*, 2007].

[5] We have expanded the initial palynological and organic geochemical data sets, and generated elemental abundances from high-resolution X-ray fluorescence (XRF) core scanning and from chemical analyses on discrete samples through upper Paleocene–lower Eocene sediments of the Expedition 302 section (cores 302-M0004A-11X through 302-M0004A-35X, from now on referred to as cores 11X through 35X). Hereby we augment previous studies [*Backman et al.*, 2006; *Brinkhuis et al.*, 2006; *Pagani et al.*, 2006b; *Sluijs et al.*, 2006] to better assess long-term late Paleocene–early Eocene environmental and climate trends, and to place the Arctic PETM record into a better constrained perspective.

2. Material and Methods

[6] Sediments from cores 35X through 27X are composed of fine-grained siliciclastic mudstone, barren of $CaCO_3$, but rich in organic matter, including palynomorphs and biomarkers [*Backman et al.*, 2006; *Sluijs et al.*, 2006; *Stein et al.*, 2006]. Cores 23X -11X are biogenic silica-rich clays, also devoid of $CaCO_3$ and rich in organic matter, including palynomorphs and biomarkers [*Backman et al.*, 2006; *Brinkhuis et al.*, 2006; *Stein et al.*, 2006].

2.1. Palynology

[7] Palynological processing was performed using standard methods [cf., e.g., *Sluijs et al.*, 2003]. Briefly, samples of 1−2 cm stratigraphic thickness were freeze or oven dried and a known amount of *Lycopodium* spores was added to ∼2−4 g of material. Samples were then treated with 30% HCl and twice with 38% HF for carbonate and silicate removal, respectively. Residues were sieved using a 15-μm nylon mesh to remove small particles. To break up clumps of residue, the sample was placed in an ultrasonic bath for a maximum of 5 min, sieved again, and subsequently concentrated into 1 mL of glycerin water, of which 10 μL was mounted on microscope slides. Slides were counted for marine (e.g., dinocysts) and terrestrial palynomorphs (e.g., pollen and spores) to a minimum of 200 dinocysts. Average sampling resolution was ∼1 m but up to 20 cm through the PETM and the total sample number is 75. Marine and terrestrial palynomorph preservation was excellent for all samples. We follow dinocyst taxonomy of [*Fensome and Williams*, 2004]. Absolute quantitative numbers were counted using the relative abundance of *Lycopodium* spores [cf. *Stockmarr*, 1972].

2.2. Inorganic Geochemistry Including XRF Core Scanning

[8] Standard analytical methods for discrete samples are discontinuous, time consuming, and expensive. Relatively fast nondestructive core logging methods yield continuous data at much finer scales (millimeter scale) than are practical for individual sampling methods [*Röhl and Abrams*, 2000]. We measured the elemental composition of sediments from Cores 19X through 35X at Bremen University, Germany, using the XRF core scanner II [*Richter et al.*, 2006; *Tjallingii et al.*, 2007]. This scanner allows high-resolution, nearly continuous, nondestructive analyses of major and minor elements at the surface of split cores. XRF data were collected every 1 cm down core over a 1 cm^2 area using 30 s count time. For the mostly laminated sediments in Core 30X [*Sluijs et al.*, 2006] we also applied a much higher resolution and collected data every 2 mm down core over a 2 mm × 1 cm area using 30 s count time. To investigate whether cyclicity in our data is related to orbital forcing we calculated spectra
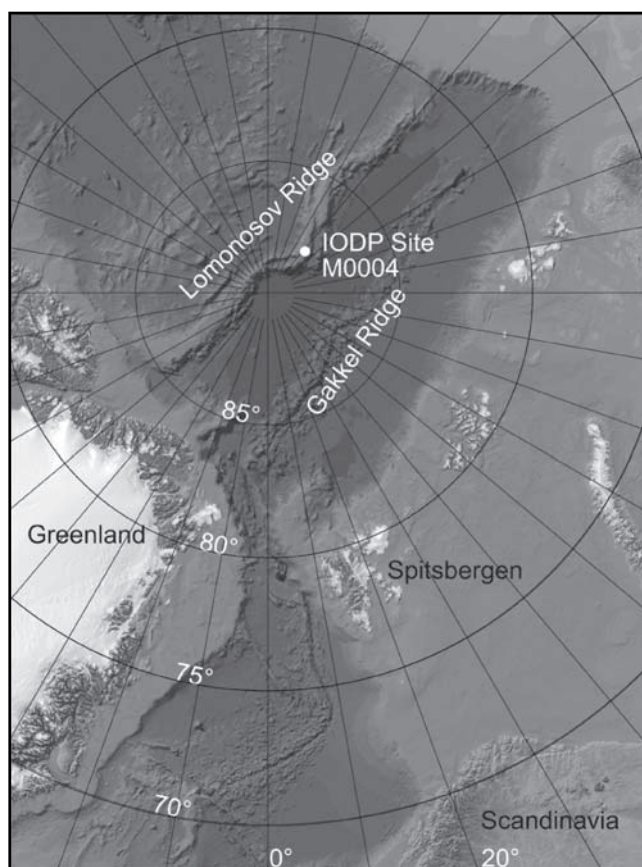
Figure 1. Bathymetric map of the Arctic Ocean showing location of Integrated Ocean Drilling Program (IODP) Site M0004 on the Lomonosov Ridge (modified from *Backman et al.* [2006]).

in the depth domain to identify the dominant cycle periods within Fe XRF scanner data of some selected cores. Blackman-Tukey power spectra have been calculated by the AnalySeries program [*Paillard et al.*, 1996].

[9] Quantitative XRF measurements were performed on 154 selected discrete samples. Sediment samples were freeze-dried and homogenized in an agate mill. All samples were analyzed for major and minor elements using a Philips PW 2400 X-ray spectrometer. 600 mg of sample was mixed with 3600 mg of a mixture of dilithiumtetraborate/lithiummetaborate (50% $Li_2B_4O_7$/50% $LiBO_2$), preoxidized at 500°C with NH_4NO_3 (p.a.), and fused to glass beads. Analytical precision and accuracy were better than 5% for all elements, as checked by in-house and international reference rocks. Total sulfur (TS) was determined using an Eltra CS 500 IR analyzer. Precision and accuracy of TS analyses were better than 3%.

2.3. Organic Geochemistry

[10] A total of 65 powdered and freeze-dried sediment samples (1−3 g dry mass) were extracted with dichloromethane (DCM)/methanol (2:1) by using accelerated solvent extraction (Dionex ACE). The extracts were separated by Al_2O_3 column chromatography using hexane/DCM

(9:1) and DCM/methanol (1:1) to yield the apolar and polar fractions, respectively. The polar fractions were analyzed for glycerol dialkyl glycerol tetraether (GDGT) lipids by high-performance liquid chromatography/mass spectrometry [*Hopmans et al.*, 2000; *Schouten et al.*, 2007a]. The relative abundance of GDGTs were used to calculate TEX_{86} [*Schouten et al.*, 2002] and TEX'_{86} [*Sluijs et al.*, 2006]; reproducibility was within ~1°C; and the Branched and Isoprenoid Tethraether (BIT) index. The BIT index describes a ratio between soil bacteria-derived and marine chrenarchaeota-derived GDGTs (see *Hopmans et al.* [2004] for more detailed method description). TEX_{86} differs from TEX'_{86} in that the latter does not include the the GDGT lipid containing three cyclopentane rings, which was unusually abundant in strata close to the PETM because of a high terrestrial GDGT component [*Sluijs et al.*, 2006]. TEX_{86} and TEX'_{86} are calibrated by core top analysis to mean annual mean SST. However, because the export of GDGT lipids to the seafloor was likely dominant during summer in the Arctic Ocean, the signal is likely skewed toward summer SSTs [*Sluijs et al.*, 2006].

2.4. Age Model

[11] Approximately 42% of the upper Paleocene and lower Eocene sediments were recovered during IODP Expedition 302 (ACEX; Cores 35X−11X) in Hole 4A on the Lomonosov Ridge (~87° 52.00′ N; 136° 10.64′ E; 1288 m water depth; Figure 1) [*Backman et al.*, 2006]. Sediments are devoid of calcareous microfossils and also barren of siliceous microfossils below ~315 m composite depth (mcd). Organic dinoflagellate cysts (dinocysts) are the only age indicative microfossils present, except for a few agglutinated benthic foraminifera [*Backman et al.*, 2006]. The lower Paleogene sediments overlie a basement of Campanian age; the unconformity occurs within Core 35X at ~405 mcd [*Backman et al.*, 2006]. The onset of the PETM is here based on identification of the CIE in both total organic carbon (TOC) and the C_{29} *n*-alkane, derived from higher plant waxes, and the occurrence of the dinocyst species *Apectodinium augustum*, which is diagnostic of the PETM [*Bujak and Brinkhuis*, 1998; *Steurbaut et al.*, 2003; *Sluijs et al.*, 2007a]. It occurs between Core 32X and the poorly recovered core catcher 31X-CC, implying a possible depth between 385.10 and 388.61 mcd [*Pagani et al.*, 2006b; *Sluijs et al.*, 2006] (Figure 2). The termination of the PETM is in general somewhat subjective for pelagic sections because of the exponential recovery of the CIE [*Röhl et al.*, 2007]. On the basis of the $\delta^{13}C$ of TOC and of C_{29} *n*-alkane, the termination of the CIE is estimated at ~378.41 mcd [*Pagani et al.*, 2006b; *Sluijs et al.*, 2006]. The position of the CIE termination is also supported by the concomitant last occurrence of the dinocyst species *Apectodinium augustum*, which has only been recorded from the CIE [*Bujak and Brinkhuis*, 1998; *Steurbaut et al.*, 2003; *Sluijs et al.*, 2007a]. As the CIE reflects an isotopic anomaly within the global exogenic carbon pool, the termination of the CIE in the Arctic organic carbon records should be synchronous with the CIE termination of well known pelagic PETM sections from the Atlantic and Pacific Oceans (e.g., [*Röhl et al.*, 2000; *Zachos et al.*, 2003,
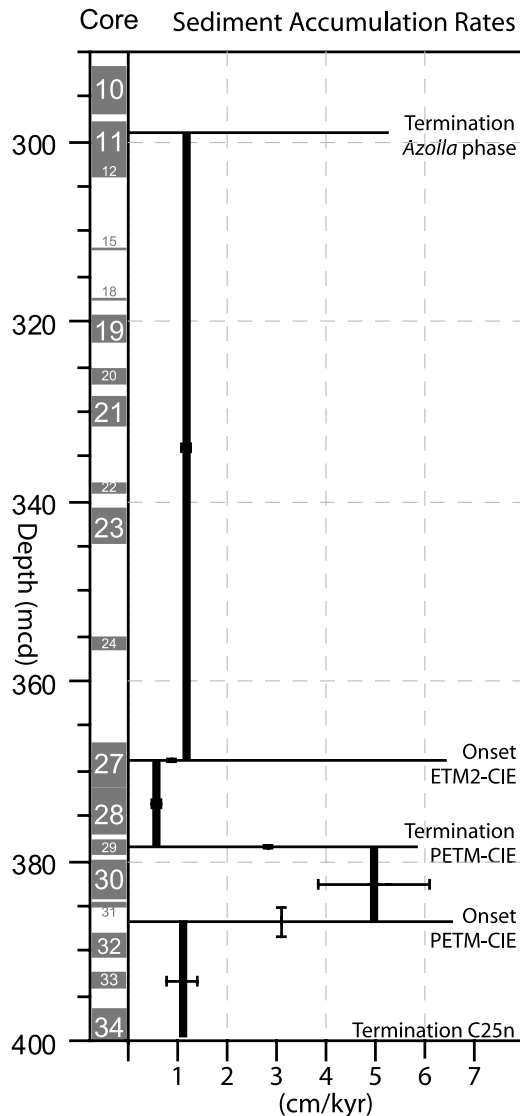
Figure 2. Core recovery and sediment accumulation rates for IODP Hole M0004A between 290 and 400 m composite depth (mcd) below seafloor. Abbreviations are ETM2, Eocene thermal maximum 2; PETM, Paleocene-Eocene thermal maximum; and CIE, carbon isotope excursion. Sedimentation rates are based on the stratigraphic thickness and the duration of time intervals (see text). Errors for the sediment accumulation rate estimates are based on the uncertainties in the stratigraphic identification of onsets and terminations of the time intervals.

2005]), even considering local factors. While the paleomagnetic signal is weak throughout the recovered section [*Backman et al.*, 2006], one clear polarity reversal was recognized at 399.63 mcd and identified as the chron C25n–C24r reversal based on the overlying PETM [*Backman et al.*, 2006].

[12] Recently, *Stein et al.* [2006] recognized a transient negative excursion in $\delta^{13}C$ of TOC at ~368 mcd, and assigned it to ETM2. This interval, however, lacked good biostratigraphic or magnetostratigraphic control and this $\delta^{13}C$ excursion could also represent another event, such as the X event. Ongoing high-resolution multiproxy studies have recorded the dinocyst species *Cerodinium wardenense* from this interval (at ~368.3 mcd) and a quasi-concomitant decrease in abundance of *Hystrichosphaeridium tubiferum* (A. Sluijs and H. Brinkhuis, unpublished results, 2007). *C. wardenense* has a reported last occurrence in the North Sea close to the nannofossil zone boundary NP10–NP11, which closely coincides with the top of the *H. tubiferum* zone of [*Bujak and Mudge*, 1994], and is just below magnetochron reversal C24r–C24n.3n [*Luterbacher et al.*, 2004]. These analogous stratigraphic characteristics, and the general similarity of early Eocene dinocyst assemblages from the Arctic Ocean and the North Sea, suggest these events are synchronous between the two oceans. Considering that the X event is dated within Chron C24n.1n and NP12 [*Röhl et al.*, 2005], and ETM2 within latest Chron C24r and earliest NP11 [*Lourens et al.*, 2005], the presence of *C. wardenense* in this interval confirms the identification of ETM2 by *Stein et al.* [2006]. The onset of the CIE of ETM2 is now recognized at 368.9 mcd (Figure 2).

[13] As yet, no other age indicative dinocysts have been recorded from the lower Eocene of the Expedition 302 cores. As indicated below, the dinoflagellate markers commonly used in the North Atlantic region were most likely not adapted to low surface water salinities that prevailed in the Arctic Ocean during this time interval. The lowermost middle Eocene is characterized by mass abundances of remains of the freshwater fern *Azolla* [*Brinkhuis et al.*, 2006]. Age-equivalent sediments with abundant *Azolla* have also been recorded at North Atlantic Ocean Drilling Program (ODP) Site 913 [*Eldrett et al.*, 2004]. The last abundant occurrence has there been calibrated to magnetochron C21r, which is also the assumed age for the top (298.9 mcd) of abundant *Azolla* fossils on Expedition 302 cores [*Brinkhuis et al.*, 2006].

[14] To ultimately estimate sediment accumulation rates, we applied the orbitally tuned, but still floating, age model defined on multiple-drilled and complete late Paleocene to early Eocene pelagic sediments from Walvis Ridge ODP Leg 208 [*Westerhold et al.*, 2007]. Owing to uncertainties in the astronomical calculations far back in geological time [*Laskar*, 1999], absolute orbitally tuned ages cannot yet be provided. Nevertheless, *Westerhold et al.* [2007] provide the most accurate durations available for intervals between the termination of Chron C25n and the onset of the CIE of the PETM (1.113 Ma), and between the onset of the PETM-CIE and the onset of the CIE of ETM2 (1.827 Ma). For the duration of the PETM-CIE, we use 170 ka, recently defined in marine pelagic sections [*Röhl et al.*, 2007], which is consistent with a revised age model from the terrestrial Bighorn Basin deposits [*Sluijs et al.*, 2007b]. For the interval between the termination of the PETM-CIE and the onset of the CIE of ETM2 we subtract 170 ka from 1.827 Ma [*Westerhold et al.*, 2007], arriving at 1.657 Ma.

[15] The age model of *Westerhold et al.* [2007] stops at the termination of chron C24r. Hence, for estimating sedimentation rates between chron C24r and the termination of the *Azolla* phase we adapt the recent geomagnetic polarity timescale of *Ogg and Smith* [2004]. The termination of the
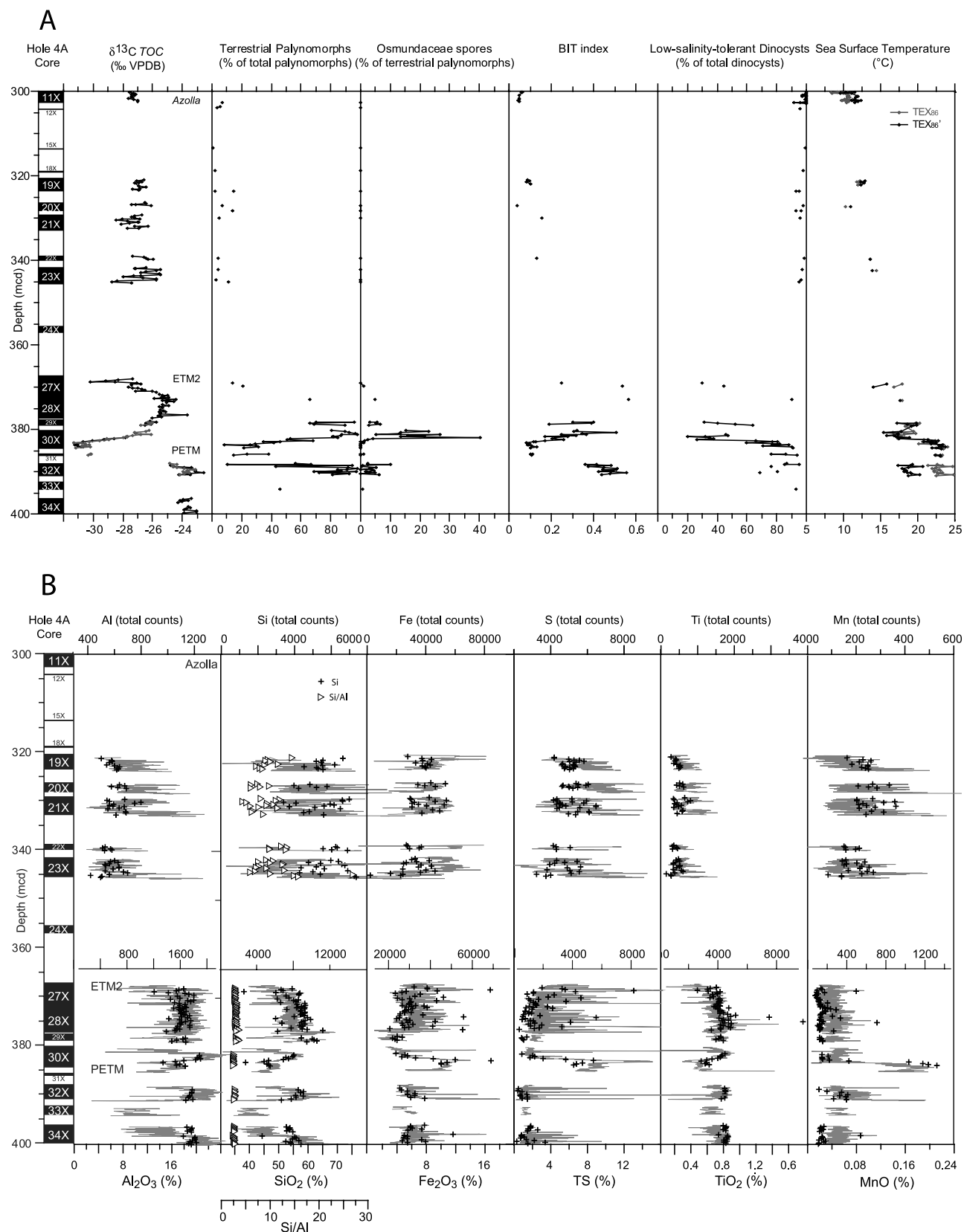
Figure 3

Table 1. Elemental Mean Values of the Upper Paleocene and Lower Eocene Part of the Integrated Ocean Drilling Program Expedition 302 Section in Comparison With Average Shale Values

	Average Above PETM (368–379 mcd)	Average Within PETM (380–391 mcd)	Average Below PETM (396–405 mcd)	Average Paleocene–Early Eocene (368–405 mcd)	Average Middle Eocene (321–346 mcd)	Average Shale[a]
Core	27X–29X	30X–32X	34X–35X	27X–35X	19X–23X	
n	54	19	31	104	50	
TOC, %	1.34	2.07	2.26	1.76	2.16	0.20[b]
TS, %	2.92	2.8	1.1	2.33	5.71	0.20[b]
Al, %	9.26	9.89	10.05	9.61	3.46	8.84
Si/Al	2.85	2.45	2.64	2.71	9.58	3.11
Ti/Al	0.051	0.045	0.052	0.05	0.042	0.053
Fe/Al	0.47	0.53	0.39	0.46	1.43	0.55
Mn/Al[c]	22	60	22	29	197	96
Mg/Al	0.162	0.148	0.125	0.148	0.273	0.18
Ca/Al	0.033	0.041	0.033	0.035	0.083	0.18
K/Al	0.27	0.229	0.235	0.252	0.211	0.34
P/Al[c]	56	76	80	67	184	79
As/Al[c]	2.7	3.3	2.4	2.7	7.2	1.1
Co/Al[c]	2	2.7	1.9	2.1	6.8	2.1
Mo/Al[c]	0.9	2.5	0.3	1	12.4	0.15
U/Al[c]	0.82	0.98	0.54	0.76	1.88	0.42
V/Al[c]	31.9	25.5	31.4	30.6	29.8	14.7
Zn/Al[c]	11.9	14.5	11.1	12.1	78.9	10.8
Zr/Al[c]	16.7	14.5	18.1	16.7	15.2	18.1
Fe/S	1.8	3.2	8.3	4.1	0.9	4.9

[a]*Wedepohl* [1971].
[b]*Brumsack* [2006].
[c]Ratio multiplied by 10^4.

Azolla phase within Chron C21r was dated at 48.6 Ma, relative to *Cande and Kent* [1995] [*Eldrett et al.*, 2004]. The timescale of *Ogg and Smith* [2004], however, has a slightly different age and duration for Chron C21r, which indicates an age of 48.1 Ma for the termination of the *Azolla* phase. The onset of Chron C24n.3n is dated at 53.8 Ma [*Ogg and Smith*, 2004], giving a duration of 5.7 Ma between the onset of C24n.3n and the termination of the *Azolla* phase. The onset of the CIE of ETM2 is 0.17 Ma older than the base of Chron C24n.3n [*Westerhold et al.*, 2007], which provides a duration of 5.90 Ma between the onset of ETM2 and the termination of the *Azolla* phase.

3. Results

### 3.1. Long-Term Late Paleocene and Early Eocene Trends

[16] Palynomorph assemblages from the upper Paleocene and lowermost Eocene (Cores 35X–27X) are characterized by abundant terrestrial palynomorphs (Figure 3a) and sediments that contain abundant amorphous organic matter, mostly of terrestrial origin. In this interval, as well as near the termination of the PETM, spores produced by the fern family Osmundaceae are consistently present and abundant (Figure 3a). Upper lower Eocene are characterized by abundant aquatic palynomorphs, notably dinocysts, and substantially lower BIT indices, while large spores derived from Osmundaceae are nearly absent (Figure 3a).
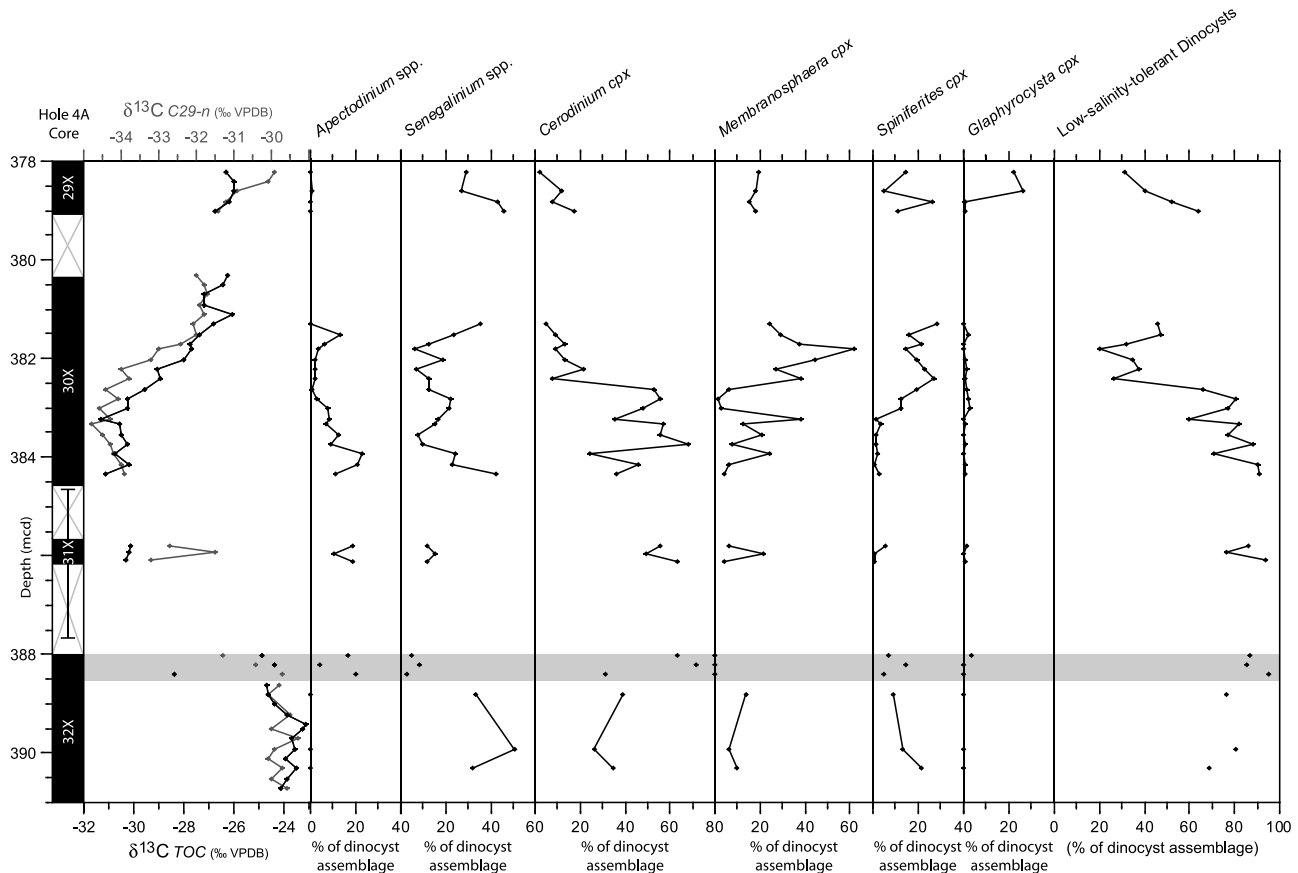
[17] Throughout the upper Paleocene and lower Eocene, dinocyst assemblages are generally dominated by the peridinioid dinocyst genera *Senegalinium* spp. and *Cerodinium* spp. Other consistently present peridinioid taxa include *Deflandrea* and *Phthanoperidinium*. These cysts were likely produced by dinoflagellates that required nutrient-rich conditions [*Dale*, 1996; *Röhl et al.*, 2004; *Sluijs et al.*, 2005] and were tolerant to low surface water salinities [*Pross and Brinkhuis*, 2005; *Brinkhuis et al.*, 2006]. In many sections, abundant occurrences of these dinocyst genera are accompanied by the records of abundant terrestrial spores and

Figure 3. Long-term trends for IODP Hole M0004A between 300 and 400 mcd. (a) Core recovery and selected palynological and organic geochemical records across the upper Paleocene and lower Eocene part of IODP Hole M0004A. The $\delta^{13}C_{TOC}$ records are from *Stein et al.* [2006] (black) and from *Sluijs et al.* [2006] (grey). Stratigraphic positions of the PETM, ETM2, and the *Azolla* phases are indicated. Core 31X was plotted 100 cm lower than mcd [*Backman et al.*, 2006] for illustration purposes. Low-salinity-tolerant dinocysts include representatives of the genera *Senegalinium, Cerodinium, Deflandrea, Lentinia, Spinidinium, Palaeocystodinium*, and *Phthanoperidinium*. (b) Geochemical element distribution across the upper Paleocene and lower Eocene part of IODP Hole M0004A: comparison of high-resolution XRF core scanning data (thin, solid lines) and chemical analyses on discrete samples (crosses indicate elements; triangles indicate elemental ratios). Because of the relatively high silica contents in cores 19X through 23X, compared to those in cores 27X through 35X, we used two slightly different X scales for illustration purposes. Core 31X was plotted 100 cm lower than mcd [*Backman et al.*, 2006] for illustration purposes.
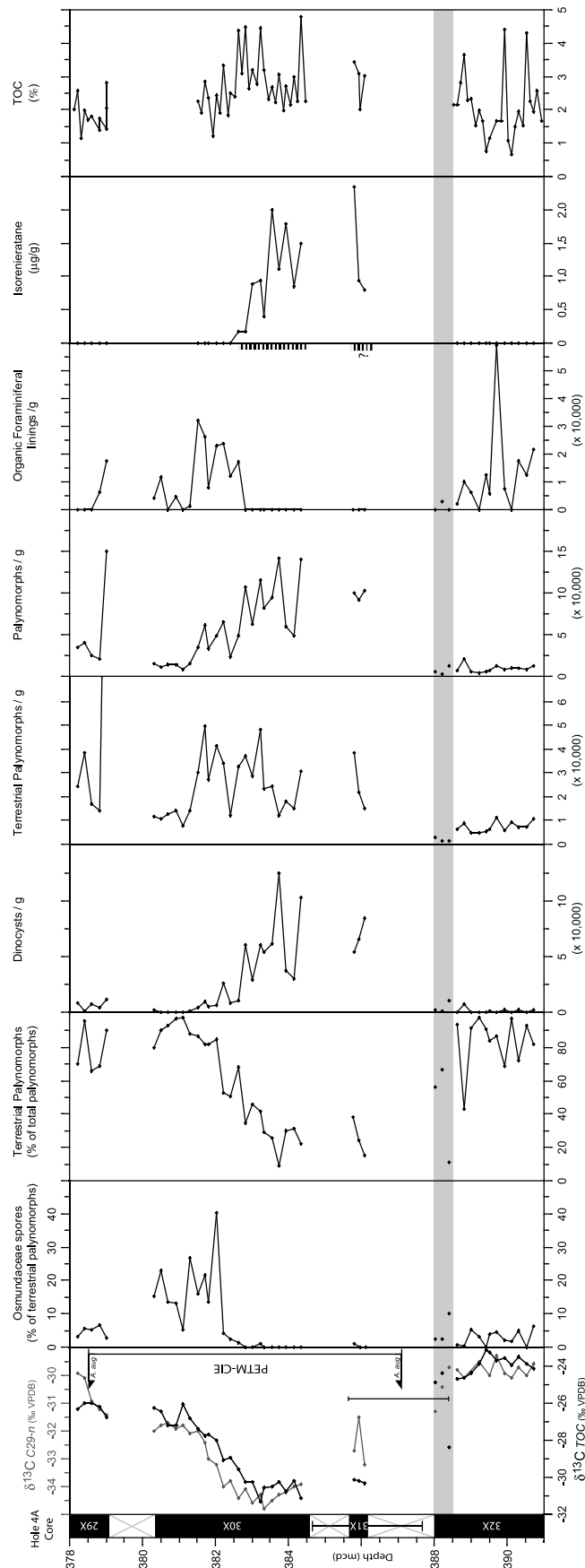
Figure 4. Core recovery and selected palynological and organic geochemical records across the PETM of IODP Hole M0004A. The $\delta^{13}C_{C29-n}$ record is from *Pagani et al.* [2006b], and the records of $\delta^{13}C_{TOC}$, percentage terrestrial palynomorphs, organic foraminiferal linings, and isorenieratane data are from *Sluijs et al.* [2006]. Total organic carbon (TOC) weight percent data are from *Sluijs et al.* [2006] and *Stein et al.* [2006]. Arrows in the $\delta^{13}C$ plot indicate first and last occurrences of dinocyst species *Apectodinium augustum* (*A. aug*). Gray bar represents the disturbed core top of core 32X black and white bars in the organic foraminiferal linings box indicate levels of laminated sediments. Core 31X was plotted 100 cm lower than mcd [*Backman et al.*, 2006] for illustration purposes.

Figure 5. Core recovery and selected dinocyst abundance records across the PETM of IODP Hole M0004A. The $\delta^{13}C_{C29\text{-}n}$ and $\delta^{13}C_{TOC}$ records are from *Pagani et al.* [2006b] and *Sluijs et al.* [2006], respectively. Grey bar represents the disturbed core top of core 32X; spp. stands for species; cpx. stands for complex. Low-salinity-tolerant dinocysts include representatives of the genera *Senegalinium*, *Cerodinium*, *Deflandrea*, *Lentinia*, *Spinidinium*, *Palaeocystodinium*, and *Phthanoperidinium*. Core 31X was plotted 100 cm lower than mcd [*Backman et al.*, 2006] for illustration purposes.

pollen, and freshwater algae [*Sluijs et al.*, 2005] and are grouped in low-salinity-tolerant dinocysts (Figures 3a). Gonyaulacoid genera include *Spiniferites*, *Areoligera* and *Membranospaera* spp.

[18] Values of the BIT index, a biomarker-based measure for the amount of river-transported soil organic matter relative to marine organic matter [*Hopmans et al.*, 2004], are relatively high at an average of ~0.4 in the upper Paleocene and lowermost Eocene, while they are low (~0.1) in the upper lower Eocene (Figure 3a). TEX$'_{86}$ records sea surface temperatures of 17° or 18°C on average in the uppermost Paleocene and lowermost Eocene, while they are 12°C to 13°C in the uppermost early Eocene.

[19] XRF core scanner data and geochemical analyses on discrete samples both clearly reflect general lithological trends. The correlation between XRF scans and single samples analyzed by conventional XRF on borate glass beads is generally good (Figure 3b). This allows geochemical element intensities (count rates) to be transferred into concentration ranges, implying a significant improvement of the resolution for the discrete sample analyses.

[20] Sediments from the upper Paleocene and lower lower Eocene are clay-rich (9.6% Al) with TOC values around 2%

(Figure 3b and fifth column of Table 1) [*Stein et al.*, 2006; *Stein*, 2007] and total sulfur contents slightly exceeding 2%. Biogenic silica is not present in significant amounts, as seen in the mean Si/Al ratio of 2.71, which is lower than the average shale value of 3.1 [*Wedepohl*, 1971; *Brumsack*, 2006]. Sediments are also devoid of $CaCO_3$, considering the very low Ca/Al ratios (fifth column of Table 1). The upper lower Eocene reveals a sediment type with a high amount of biogenic silica (Si/Al ratio averaging three times the shale level) and extremely high Fe and S contents (sixth column of Table 1 and Figure 3b). The sediments are fully pyritized (Fe/S < 1), have high trace element concentrations and are enriched in diagenetic minerals like apatite or rhodochrosite resp. ankerite (higher Ca/Al, P/Al, and Mn/Al ratios), owing to significantly more pore space [*Backman et al.*, 2006].

3.2. Paleocene-Eocene Thermal Maximum

[21] The number of total palynomorphs per gram of dry sediment is particularly high within the lower part of the PETM (Figure 4) and relatively low before and after the PETM. The same holds for the number of dinocysts per gram sediment. Dinocyst diversity across the PETM is low compared to other sites [e.g., *Powell et al.*, 1996; *Crouch et*
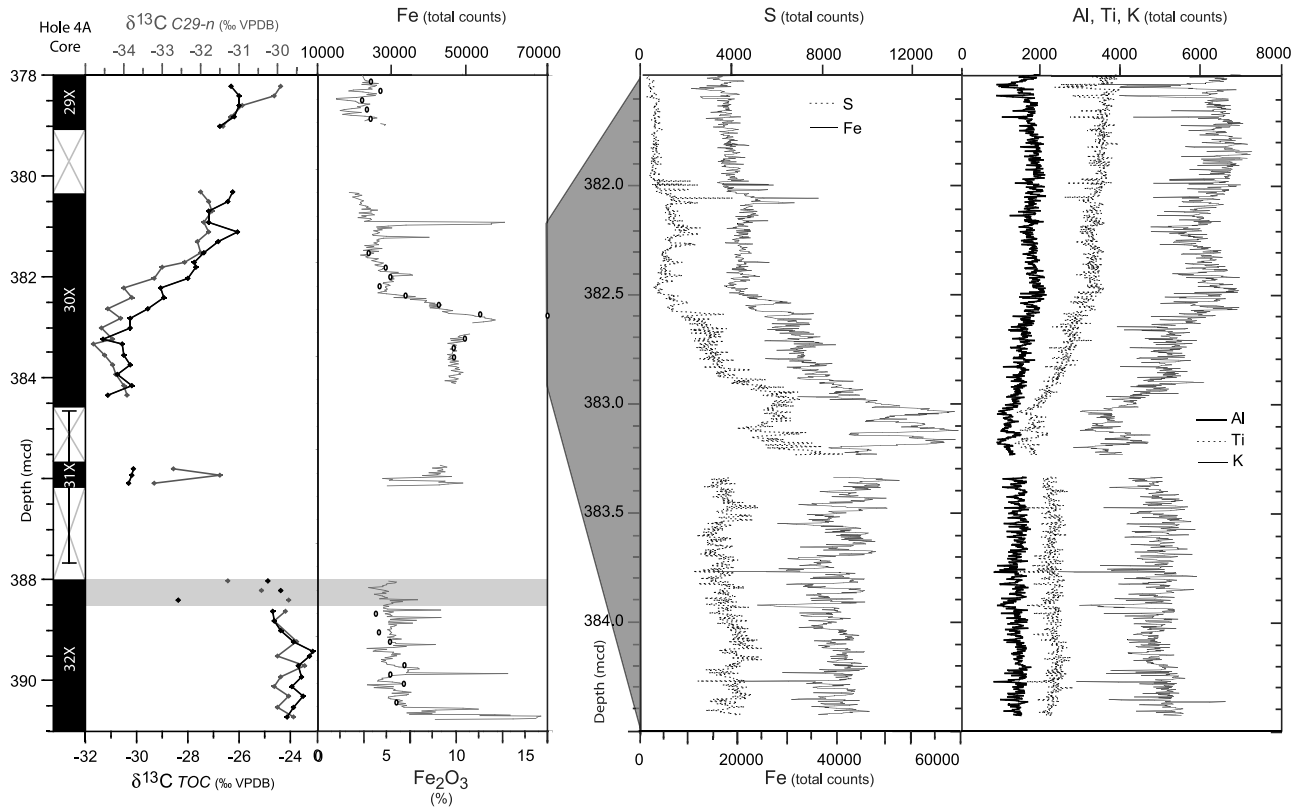
Figure 6. (left) Core recovery and Fe data across the PETM of IODP Hole M0004A plotted alongside the CIE based on $\delta^{13}C_{C29-n}$ and $\delta^{13}C_{TOC}$. The $\delta^{13}C_{C29-n}$ and $\delta^{13}C_{TOC}$ records are from *Pagani et al.* [2006b] and *Sluijs et al.* [2006], respectively. (right) S, Fe, Al, Ti, and K data for laminated core 302-M0004A-30X in 2-mm resolution. See text for further explanation. Grey bar represents the disturbed core top of core 32X. Core 31X was plotted 100 cm lower than mcd [*Backman et al.*, 2006] for illustration purposes.

al., 2003; *Crouch and Brinkhuis*, 2005] and apart from *Apectodinium* [*Sluijs et al.*, 2006], assemblages in the lower part of the PETM are dominated by *Cerodinium* (Figure 5). Although consistently present before and during the initial stages of the PETM, normal marine taxa belonging to the *Membranosphaera* complex (cpx; consisting of the genera *Membranosphaera*, *Histiocysta* and *Microdinium*) and *Spiniferites* cpx (consisting of the genera *Spiniferites*, *Achomosphaera*, *Hafniasphaera* and *Rottnestia*) become abundant toward the termination of the PETM (Figure 5). Above the PETM, typical open marine inner neritic [*Brinkhuis*, 1994; *Pross and Brinkhuis*, 2005; *Sluijs et al.*, 2005] *Glaphyrocysta* cpx (consisting of the genera *Glaphyrocysta* and *Areoligera*) become more abundant, particularly *Glaphyrocysta ordinata* (Figure 5). Other more or less consistently present taxa from the PETM interval include *Caligodinium aceras, Diphyes colligerum, Alisocysta* sp.2 of *Heilmann-Clausen* [1985], *Hystrichosphaeridium tubiferum, Muratodinium fimbriatum, Operculodinium* spp., *Thalassiphora pelagica, T. delicata* and *Wilsonidium tesselatum*.

[22] During the PETM an increase in S, Fe/S, Fe/Al, Mn/Al, and trace element/Al ratios is recorded (Table 1 and Figure 3b). Si/Al and Ti/Al ratios are low during the PETM, whereas the Fe/Al ratio is slightly elevated. A distinct Fe maximum was identified in both XRF data sets at ~383 mcd (Figure 6).

4. Discussion

4.1. Sediment Accumulation Rates

[23] Sediment accumulation rates are estimated for the uppermost Paleocene and lower Eocene of the IODP Expedition 302 section using depths and durations as described above (Figure 2). Generally, sediment accumulation rates are close to 1 cm ka^{-1}, but are significantly higher (5.0 ± 1.2 cm ka^{-1}) during the PETM (Figure 2). While there is notable uncertainty in this estimate due to the imprecise position of the onset of the PETM-CIE, it, nevertheless, implies that sedimentation accumulation rates increased threefold to fivefold during the PETM. This was most likely a result of enhanced siliciclastic input by rivers in response to an intensification of the hydrological cycle during the PETM, which is also supported by changes in geochemical data, such as Fe/Al ratios (Table 1), and biotic changes (see below).

4.2. Changes in Relative Sea Level

[24] On the basis of palynological and geochemical records, upper Paleocene to lower Eocene sediments from Expedition 302 Hole M0004A can generally be divided in two major intervals, that is, upper Paleocene through lower lower Eocene (Cores 35X–27X, at ∼400–365 mcd) and upper lower Eocene (Cores 24X–12X, at ∼365–310 mcd) (Figure 3).

[25] In the upper Paleocene and lowermost Eocene, as well as near the termination of the PETM, spores produced by the fern family Osmundaceae are consistently present and abundant (Figure 3a). These spores are very large and thick-walled (100–300 μm) and cannot have been transported over long distances, implying the site was close to shore. As the spreading Gakkel Ridge had separated the Lomonosov Ridge from the Siberian Shelf by the latest Paleocene [Jokat et al., 1992, 1995], the consistent occurrence of Osmundaceae spores indicates that parts of the Lomonosov Ridge in the vicinity of the drill site were still above sea level at least until near the onset of ETM2 (Figure 3a). This interpretation is supported by the general abundance of terrestrial palynomorphs and palynodebris and high BIT index values (Figure 3a).

[26] A marine transgression in the lower part of the PETM was initially suggested by Sluijs et al. [2006], based on a relative decrease in terrestrially derived organic matter recorded in palynomorph assemblages, BIT index and Rock Eval Hydrogen Index. Corroborating this interpretation is the near absence of Osmundaceae spores during most of the PETM (∼387–382 mcd; Figure 4). As discussed above, these large spores are not likely to be transported over long distances and we surmise that during the initial stages of the PETM the site was located too far from shore for the spores to have been deposited. Dinocyst assemblages were barely influenced by changes in sea level but largely reflect changes in salinity and runoff (see below).

[27] Upper lower Eocene strata are characterized by low abundances of terrestrially derived organic matter (few terrestrial palynomorphs low BIT values, and the absence of Osmundaceae spores; Figure 3a). Hence it appears that during the late early Eocene the drill site was located further from shore than during the late Paleocene–earliest Eocene, which most likely reflects the gradual subsidence of the Lomonosov Ridge during the early Eocene (M. O'Regan et al., Mid-Cenozoic tectonic and paleoenvironmental setting of the central Arctic Ocean, submitted to Paleoceanography, 2007).

4.3. Salinity and Runoff

[28] In the upper lower Eocene, very high percentages of low-salinity-tolerant dinocysts are recorded (Figure 3a), despite the more distal setting relative to underlying Upper Paleocene to lowermost Eocene. In addition, dinocyst diversity is low and very few typically open marine dinocysts (e.g., Spiniferites, Areoligera and Membranospaera spp.) are recorded. Dinocyst assemblages in this interval are very similar to those recorded in the interval characterized by abundant remains of the freshwater fern Azolla, near the top of the lower Eocene [Brinkhuis et al., 2006]. This indicates that brackish or fresh surface waters already

persisted during the upper lower Eocene, suggesting that only a small decrease in salinity or a change in another critical environmental parameter, perhaps phosphorus concentrations, caused the inception of conditions favorable for massive Azolla growth.

[29] The trend from nearly 100% low-salinity-tolerant dinocyst taxa during the lower part of the PETM to assemblages dominated by typical marine taxa, such as Membranosphaera, Spiniferites and Glaphyrocysta, toward the termination of the PETM, and after, likely reflects an increase in surface salinity. This interpretation is consistent with the concomitant termination of photic zone euxinia, indicated by the decrease and subsequent absence of isorenieratane [Koopmans et al., 1996] (Figure 4), suggesting a less stratified water column, and δD-reconstructed surface water salinities [Pagani et al., 2006b] during the recovery phase of the PETM.

[30] The number of palynomorphs and dinocysts per gram of dry sediment is particularly high within the lower part of the PETM (Figure 4). This is likely, at least in part, associated with enhanced runoff as a climate response during the PETM [Pagani et al., 2006b; Sluijs et al., 2006]. This increased nutrient supply to surface waters, resulting in more dinocyst production, and transported more terrestrial palynomorphs into the basin. Alternatively, absolute quantitative numbers, particularly dinocysts, are highest within the laminated interval (∼387–382.5 mcd), which also contains isorenieratene derivatives indicating photic zone euxinia (Figure 5). This suggests that despite the good palynomorphs preservation throughout the whole section, preservation may have affected absolute palynomorph concentrations. However, the influence of preservation may have been minimal given that terrestrial palynomorph concentrations remain unaffected at the termination of water column anoxia at ∼382.5 mcd (Figure 4).

4.4. Temperature Trends

[31] Dinocyst assemblages throughout the upper Paleocene and lower Eocene consist of previously described cosmopolitan taxa. Strong temperature-forced biogeographical partitioning of dinocyst assemblages, such as recorded during modern [Rochon et al., 1999; de Vernal et al., 2001; Marret and Zonneveld, 2003] and glacial periods [de Vernal et al., 2002, 2005], and the middle to late Eocene of the Southern Ocean [Wrenn and Beckmann, 1982; Brinkhuis et al., 2003; Sluijs et al., 2003; Huber et al., 2004; Stickley et al., 2004; Warnaar, 2006], was not present during the upper Paleocene and lower Eocene. This indicates that Arctic Ocean surface temperatures were warm enough for cosmopolitan, and during the PETM even subtropical species to be present and not cool enough to develop an Arctic endemic assemblage.

[32] This biogeographic observation is consistent with the very warm TEX'_{86}-reconstructed sea surface temperatures during the late Paleocene and early Eocene, which during the PETM peaked at ∼23°C [Sluijs et al., 2006] (Figures 3a and 4). Such temperatures are also consistent with previous late Paleocene and early Eocene temperature estimates for the Arctic realm, based on other marine and terrestrial proxies [Greenwood and Wing, 1995; Bice et al., 1996;

Markwick, 1998; *Tripati et al.*, 2001]. Recently, TEX_{86} and planktonic foraminifer $\delta^{18}O$ data from Tanzania have indicated tropical temperatures of at least 30°C–33°C for this time period [*Pearson et al.*, 2007], which implies that the equator-to–North Pole surface temperature gradient, at least for boreal summer, was composed of only ~15°C. This agrees with other studies that have noted reduced meridional temperature gradient during late Paleocene–early Eocene greenhouse climates [*Zachos et al.*, 1994; *Fricke and Wing*, 2004; *Sluijs et al.*, 2006], which cannot be simulated by current generation fully coupled general circulation models [*Shellito et al.*, 2003; *Huber and Nof*, 2006; *Sluijs et al.*, 2006].

[33] Arctic Ocean surface temperatures during the late early Eocene appear to have been ~4°C lower than during the late Paleocene and earliest Eocene (Figure 3a). This result differs the general assumption that climate during the late early Eocene was warmer than during late Paleocene and earliest Eocene [e.g., *Zachos et al.*, 2001]. A possible scenario is that the Arctic region did not follow this global trend. Quantitatively, such a cooling of the Arctic Ocean is consistent with the stagnation of ocean heat transport from lower latitudes [*Huber and Sloan*, 2001; *Huber et al.*, 2003; *Huber and Nof*, 2006], which could have been established through a decrease of oceanic exchange between the Arctic and adjacent oceans [cf. *Brinkhuis et al.*, 2006]. This scenario would be consistent with the recorded 100% low-salinity-tolerant dinocyst assemblages, as a decrease in ocean exchange with adjacent oceans would also limit salt transport into the Arctic Ocean. Alternatively, the recorded early Eocene sea surface cooling trend could be attributed to local effects, such as the more distal position relative to the coast and a slightly deeper setting.

4.5. Environmental Implications of the *Apectodinium* Acme

[34] Prior to the PETM, the genus *Apectodinium* was only locally and periodically abundant at low latitudes, while during the PETM it became dominant and made up >40% of the dinocyst assemblage on a global scale [*Heilmann-Clausen*, 1985; *Powell et al.*, 1996; *Bujak and Brinkhuis*, 1998; *Heilmann-Clausen and Egger*, 2000; *Crouch et al.*, 2001, 2003; *Egger et al.*, 2003; *Sluijs et al.*, 2006, 2007a, 2007b]. In the Arctic Ocean during the PETM, *Apectodinium* is slightly less abundant, making up ~20% of the assemblage. Typical low-salinity-tolerant dinocysts are dominant. A similar trend is recorded on the New Jersey Shelf, where *Apectodinium* became outnumbered by typical low-salinity-tolerant dinocysts during the PETM [*Sluijs et al.*, 2007a]. This indicates that, while *Apectodinium* was successful at low salinities other taxa were able to dominate dinocyst assemblages under such ecological conditions. Given the low-latitude preference of *Apectodinium*, it must have required high temperatures [*Bujak and Brinkhuis*, 1998; *Crouch et al.*, 2001], perhaps a minimum of 20°C [*Sluijs et al.*, 2006, 2007a]. In addition to temperature, *Apectodinium* perhaps required stratified surface waters [*Crouch et al.*, 2003]. Moreover *Apectodinium* has morphological characteristics identical to cysts of modern heterotrophic dinoflagellates, which has fueled the hypothesis that *Apectodinium*

was a heterotrophic dinoflagellate [*Bujak and Brinkhuis*, 1998]. Basic predator-prey abundance models indicate that with higher nutrient supplies, ecosystems should become relatively enriched in organisms that are higher up in the food chain, i.e., heterotrophic. Increasing nutrient levels may therefore have contributed to the *Apectodinium* acme. If so, the global character of the acme implies that at least neritic and coastal settings underwent significant eutrophication on a global scale [*Bujak and Brinkhuis*, 1998; *Crouch et al.*, 2001], a hypothesis corroborated by many proxy data (see overview of *Sluijs et al.* [2007b]). For the Arctic region, this interpretation is consistent with enhanced nutrient input by rivers, higher TOC concentrations, and productivity-related trends in the algal-derived C_{17} n-alkane [*Pagani et al.*, 2006b]. Modern dinoflagellate blooms usually last for several days to weeks [e.g., *Dale*, 1996]. Conceivably, *Apectodinium* blooms during the PETM had similar dynamics, in which case the *Apectodinium* acme would imply a change in specific seasonal conditions of surface waters. This may include any of the above environmental factors. However, even a combination of these factors was likely not truly unique in the early Paleogene, suggesting that some critical environmental factor that stimulated massive *Apectodinium* production has not yet been identified.

4.6. Water Column and Seafloor Oxygenation

[35] Previous studies in the Arctic region have concluded that bottom waters were at least temporally devoid of oxygen, based on laminated sediments, the absence of fossils of benthic organisms and organic geochemical evidence such as biomarkers [*Backman et al.*, 2006; *Brinkhuis et al.*, 2006; *Sluijs et al.*, 2006; *Stein et al.*, 2006]. Moreover, photic zone euxinia developed during the PETM [*Sluijs et al.*, 2006]. To further assess the evolution of bottom water oxygenation we apply XRF analyses.

[36] In sediments from the upper Paleocene and lower lower Eocene, sulfur is very abundant and the redox sensitive major elements Fe and Mn are present in concentrations slightly (Fe) or significantly (Mn) below the average shale level, in accordance with a generally reducing suboxic paleoenvironmental setting. This is also reflected in elevated As/Al, Mo/Al, U/Al, and V/Al ratios (Table 1). The Fe/S ratio is, however, significantly higher than 1, which points toward incomplete pyritization of this sequence, either because of a lack of seawater sulfate or, less likely, enhanced sedimentation rates [e.g., *Rachold and Brumsack*, 2001] (Figure 2).

[37] During the mid early Eocene the clay-rich mudstones are replaced by biogenic silica-rich sediments (Si/Al ratio averaging three times the shale level). High trace element/Al ratios also point toward euxinic conditions, possibly comparable to Modern deep water conditions in the Baltic Sea [*Huckriede and Meischner*, 1996].

[38] An additional advantage of combining XRF scanning and discrete sample analyses is that it may be possible to distinguish real changes in composition from the effects of end-member mixing. For example, the Ti or TiO_2 spikes recorded in Core 28X (~375 mcd) are possibly associated with ash layers. While turbidites could be an alternative explanation, these are normally characterized by a coarse-
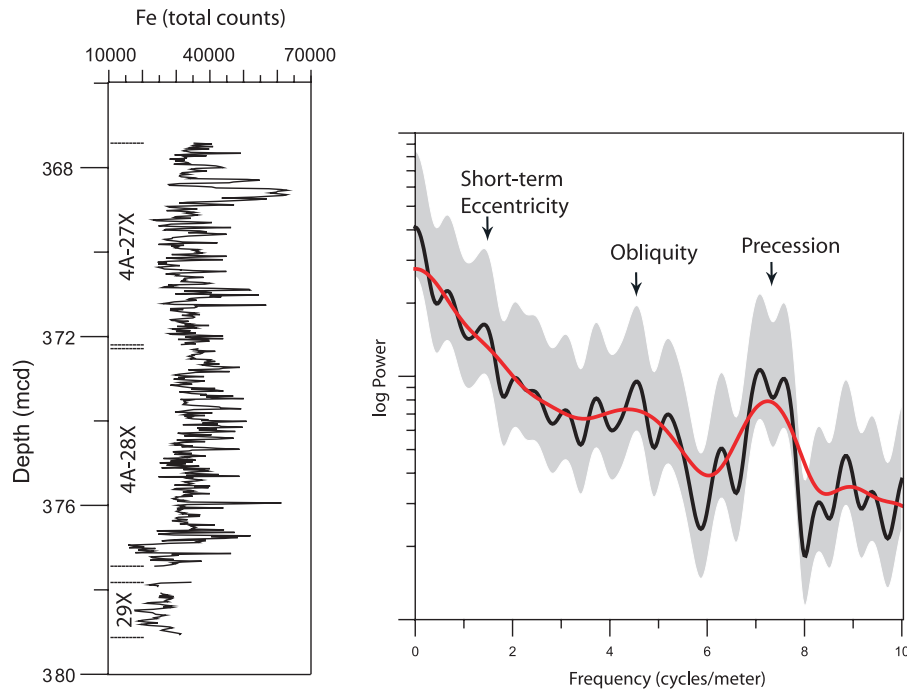
Figure 7. (left) Fe record of cores 302-M0004A-27X- to 302-M0004A-29X exhibiting orbital cyclicity (mainly precession cycles and their eccentricity modulation) in early Eocene sediments. (right) Spectral analysis for CORES 302-M0004A-27X and 302-M0004A-28X, excluding data of the ETM2 interval. Prior to spectral analysis the data were detrended and normalized. Blackman-Tukey power spectra (bold black line) have been calculated by the AnalySeries program [*Paillard et al.*, 1996] using 80% confidence interval (grey area, 30% of series); background noise was estimated (10% of series); bold red line is the estimated background noise (10% of series). Bandwidth (0.58) and confidence limits are based on a Bartlett window with a number of lags that equal 30% of the length of the data series.

grained base, and sudden increases in elemental concentrations resulting into asymmetric Ti distributions. The high-resolution XRF scans do not exhibit sharp increase of Ti counts, but rather symmetrical peaks, so turbidite layers can most likely be excluded.

[39] The occurrence of laminated sediments, from Core 31X at the onset of the PETM to 382.5 mcd, implies the absence of bioturbating organisms. This is corroborated by the absence of benthic foraminiferal linings, which are present below and above the laminated interval (Figure 4). Together, this suggests bottom waters became depleted in oxygen during the PETM. Within the laminated interval, derivatives of the characteristic pigment isorenieratene, derived from the brown strain of photosynthetic green sulfur bacteria, are recorded (Figure 4). These bacteria require euxinic (anoxic and sulfidic) conditions to thrive [*Sinninghe Damsté et al.*, 1993], which implies that during the lower part of the PETM photic zone euxinia developed at the drill site coincident with bottom water anoxia [*Sluijs et al.*, 2006]. This can be explained by increased surface ocean stratification due to enhanced Arctic precipitation and runoff; a hypothesis corroborated by hydrogen isotope data [*Pagani et al.*, 2006b; *Sluijs et al.*, 2006], a threefold to fivefold increase in sediment accumulation rates (Figure 2) and increased concentrations of terrestrial and marine palynomorphs (Figure 4).

[40] The XRF data support a scenario of reduced oxygenation during the PETM (second, third, and fourth columns of Table 1 and Figure 6). The section below the PETM (405 to 396 mcd; fourth column of Table 1) is relatively low in S, Fe/Al, Mn/Al, and trace element/Al ratios. This suggests less intense reducing conditions and possibly low pyritization. During the PETM, conditions were much more reducing, as reflected in higher pyritization (higher Fe/S ratio, higher S contents) and elevated trace element/Al ratios. Interestingly, Si/Al and Ti/Al ratios are low during the PETM, whereas the Fe/Al ratio is slightly elevated. This may indicate more intense weathering, which also correlates with the high percentages of low-salinity-tolerant dinocysts (Figure 5), and a shift toward Al-rich (possibly kaolinite) and Fe-rich terrigenous detrital input.

[41] A distinct Fe maximum was identified in both XRF data sets at ∼383 mcd (Figure 6). This is a critical horizon, as it marks the onset of the recovery of the CIE in both $\delta^{13}C_{TOC}$ and $\delta^{13}C_{C29-n}$ and the termination of the strictly laminated interval (Figure 4). Fe/S ratios are above unity in many samples from Core 30X (Table 1), pointing toward incomplete pyritization. This could be due to various reasons, such as a lack of sulfate (i.e., insignificant seawater influence), a lack of organic matter to metabolize (which is rather unlikely considering the high TOC content), or very high sedimentation rates. On the basis of high-resolution

scans we see a reflection of this phenomenon from 383.0–383.2 mcd (Figure 6), where a triple peak in Fe counts is not accompanied by peaks in S counts. This may indicate the presence of a significant amount of freshwater, which would provide the required Fe, but is low in sulfate. This interval may represent an almost freshwater environment, which also agrees with the palynomorph assemblages, BIT index and Rock Eval Hydrogen Index data [*Sluijs et al.*, 2006].

4.7. Orbital Forcing of Sedimentary Cycles

[42] It has been widely accepted that XRF measurements usually show a significantly higher signal-to-noise ratio and a more consistent hole-to-hole agreement than any of the shipboard physical property measurements (e.g., density, color reflectance, magnetic susceptibility), and are therefore a great archive for time series analysis of relatively complete sections [*Pälike et al.*, 2001; *Röhl et al.*, 2003, 2004; *Jaccard et al.*, 2005; *Tjallingii et al.*, 2007; *Westerhold et al.*, 2007]. While the uppermost Paleocene and lower Eocene just represents an incompletely recovered section (Figure 2) [*Backman et al.*, 2006], the XRF scans for the recovered cores provide a suitable data set to further investigate the details of climatic signals in the record [*Pälike et al.*, 2008; D. Spofforth et al., Palaeogene record of elemental concentrations in sediments from the Arctic Ocean obtained by XRF analyses, submitted to *Paleoceanography*, 2007]. Owing to the limited core recovery we restricted the time series analysis to the adjacent cores 27X and 28X (Figure 7) and removed the ETM2 horizon from the data in order to avoid spectral analysis disturbance. Early Eocene sediments between the PETM and ETM2 are meanwhile well known from other sections, such as the ODP Leg 208 sites [*Lourens et al.*, 2005; *Westerhold et al.*, 2007] and ODP Site 1051 [*Cramer et al.*, 2003; *Röhl et al.*, 2003], and therefore good control exists on the total duration of the interval. Spectral analyses of the interval prior to ETM2 (Figure 7) reveal related frequencies of the dominant cycles at 1.45, 4.5, and 7.1–7.6 cycles per meter which equal 0.7, 0.26, and 0.13–0.14 m cycle^{-1}. The periodicities have a nearly perfect 1:2.5:5 frequency ratio and are diagnostic for a combination of the short (100 ka) eccentricity cycle, weak obliquity cycle (41 ka), but an especially pronounced and split precession (23.7 ka, 22.4 ka) cycle. This provides robust evidence for a match of the sedimentary rhythm to orbital forcing and a dominance of precession cycles modulated by eccentricity.

4.8. Organic Carbon Sequestration in the Arctic During the PETM?

[43] As discussed above, sediment accumulation rates during the PETM increased threefold to fivefold, while on average wt % TOC are approximately 1% higher during the PETM (2.8%) than just prior to the PETM (~2.0%; Figure 4). If we assume that anoxic conditions, along with high TOC concentrations, and elevated sedimentation rates were a basin-wide phenomenon, we can roughly estimate the scale of excess organic carbon burial. For this purpose we calculate the amount of organic carbon buried per 1000 years on the Lomonosov Ridge prior to and during the PETM, using % TOC, bulk density and above sedimentation rates. Given a bulk sediment density of 1.3 g cm^{-3} [*Backman et*

al., 2006], sediment accumulation rates of 1.2 cm ka^{-1} and an average TOC content of 2.0 wt %, late Paleocene organic carbon burial rates at the drill site approximated 0.30 g C m^{-2} a^{-1}. During the PETM, with a similar bulk sediment density [*Backman et al.*, 2006], sediment accumulation rates of 5.0 cm ka^{-1} and an average TOC content of 2.8 wt %, carbon burial rates at the drill site approximated 1.81 g C m^{-2} a^{-1}. This implies that organic carbon accumulation rates increased sixfold during the PETM. This increase was probably partly caused by improved preservation of organic matter because of anoxic conditions in the lower photic zone and on the seafloor. Moreover, marine productivity likely increased, as suggested by elevated numbers of dinocysts per gram of sediment (Figure 4) despite increased sedimentation rates (Figure 2), and trends in the δ^{13}C of algal-derived C$_{17}$ n-alkane [*Pagani et al.*, 2006b].

[44] The excess carbon burial during the PETM at the drill site approximated 1.51 g C m^{-2} a^{-1}. Assuming a 170-ka duration of the CIE of the PETM [*Röhl et al.*, 2007; *Sluijs et al.*, 2007b], and that the estimated rates are valid for the entire 3,000,000 km^2 Arctic Ocean, the excess burial of organic carbon was on the order of 770 Gt for the PETM. For comparison, a similar amount of carbon derived from methane hydrates is estimated to be required to generate the entire CIE in the global exogenic carbon pool [*Dickens et al.*, 1995; *Dickens*, 2001].

[45] We realize many uncertainties could compromise this calculation, such as the missing (exact) detailed correlation of the termination of the CIE to the deep marine record on which the 170 ka duration is based [*Röhl et al.*, 2007], the exact size of the Arctic sedimentary basin, or the hypothesis that organic carbon burial changed similarly throughout the entire Arctic basin. However, this estimate for excess organic carbon burial during the PETM should be within an order of magnitude of the real burial. Additionally, organic-rich PETM successions have been recorded from the Tethyan realm [*Bolle et al.*, 2000; *Crouch et al.*, 2003; *Gavrilov et al.*, 2003]. This indicates that not only carbonate burial [*Zachos et al.*, 2005; C. M. John et al., Continental margin records of the Paleocene-Eocene thermal maximum: Implications for global carbon cycle and hydrological cycling, submitted to *Paleoceanography*, 2007], but also organic carbon burial in the Arctic and other restricted marine areas may have played a quantitatively important role in the sequestration of injected carbon during the PETM. Interestingly, this should have dampened the magnitude and perhaps the duration of the CIE in sedimentary carbon by increasing the organic versus inorganic carbon burial ratio. This would suggest that injected ^{13}C-depleted carbon was even more depleted than assumed or that the volume of injected carbon was larger than has been estimated using δ^{13}C analyses only [*Dickens et al.*, 1995; *Dickens*, 2000, 2001; *Cramer and Kent*, 2005; *Higgins and Schrag*, 2006; *Pagani et al.*, 2006a; *Schouten et al.*, 2007b].

5. Conclusions

[46] We reconstruct long-term latest Paleocene and early Eocene (~57–50 Ma) environmental and climate trends in

the Arctic Ocean, and focus on the Paleocene-Eocene thermal maximum (PETM) (~55 Ma), using strata recovered from the Lomonosov Ridge by Integrated Ocean Drilling Program Expedition 302. Palynological and organic geochemical data suggest the drill site was close to shore during the latest Paleocene and early early Eocene and that parts of the Lomonosov Ridge were still subaerial. The site became located farther from shore during the late early Eocene, likely related to gradual subsidence of the Lomonosov Ridge. Organic dinoflagellate cyst (dinocyst) assemblages point to brackish and productive surface waters throughout the latest Paleocene and early Eocene. This suggests that low salinities in the Arctic surface waters were already prevalent prior to freshwater conditions that prevailed during the mass growth of the hydropterid fern *Azolla* during the earliest middle Eocene. Dinocyst assemblages are cosmopolitan throughout the latest Paleocene and early Eocene, suggesting warm sea surface temperatures, which is corroborated by TEX$'_{86}$-reconstructed values of $14°-18°C$.

[47] Sediments from the upper Paleocene and lower lower Eocene are clay- and organic-rich without biogenic silica and XRF analyses show that total sulfur contents slightly exceed 2%, reflecting reducing conditions within the sediment. For the upper lower Eocene high trace element/Al ratios furthermore point toward euxinic conditions, possibly comparable to the Modern deep waters in the Baltic Sea.

[48] The presence of ETM2 in the IODP Expedition 302 cores is confirmed by dinocyst stratigraphy. Spectral analysis reveals that the cyclicity, recorded in XRF scanning Fe data from early Eocene strata close to ETM2 is related to precession.

[49] During the PETM bottom waters become more reducing, based on elevated sulfur and Fe/Al, Mn/Al, and trace element/Al ratios. Element ratios further evidence more intense weathering and a shift toward Al-rich (possibly kaolinite) and Fe-rich terrigenous detrital input. This is corroborated by a strong increase in sediment accumulation rates during the PETM, as well as higher absolute abundances of dinocysts (low-salinity-tolerant taxa) and terrestrial palynomorphs per gram of sediment. Our evidence supports a sea level rise across the onset of the PETM at this site. Finally, on the basis of total organic carbon content and variations in sediment accumulation rates, excess burial of organic carbon in the Arctic Ocean appears to have been quantitatively significant during the PETM and potentially contributed to the sequestration of the injected carbon.

References

Adams, C. G., D. E. Lee, and B. R. Rosen (1990), Conflicting isotopic and biotic evidence for tropical sea-surface temperatures during the Tertiary, *Palaeogeogr. Palaeoclimatol. Palaeoecol.*, *77*, 289–313.

Archer, D. (2005), Fate of fossil fuel CO_2 in geologic time, *J. Geophys. Res.*, *110*, C09S05, doi:10.1029/2004JC002625.

Backman, J., K. Moran, D. B. McInroy, L. A. Mayer, and Expedition-Scientists (2006), *Proceedings of the Integrated Ocean Drilling Program*, vol. 302, Integr. Ocean Drill. Program Manage. Int., Inc., College Station, Tex.

Bice, K. L., M. A. Arthur, and L. Marincovich Jr. (1996), Late Paleocene Arctic Ocean shallow-marine temperatures from mollusc stable isotopes, *Paleoceanography*, *11*, 241–250.

Bolle, M.-P., A. Pardo, K.-U. Hinrichs, T. Adatte, K. von Salis, S. Burns, G. Keller, and N. Muzylev (2000), The Paleocene-Eocene transition in the marginal northeastern Tethys (Kazakhstan and Uzbekistan), *Int. J. Earth Sci.*, *89*, 390–414.

Bowen, G. J., W. C. Clyde, P. L. Koch, S. Y. Ting, J. Alroy, T. Tsubamoto, Y. Q. Wang, and Y. Wang (2002), Mammalian dispersal at the Paleocene/Eocene boundary, *Science*, *295*, 2062–2065.

Brinkhuis, H. (1994), Late Eocene to early Oligocene dinoflagellate cysts from the Priabonian type-area (northeast Italy): Biostratigraphy and palaeoenvironmental interpretation, *Palaeogeogr. Palaeoclimatol. Palaeoecol.*, *107*, 121–163.

Brinkhuis, H., S. Sengers, A. Sluijs, J. Warnaar, and G. L. Williams (2003), Latest Cretaceous-earliest Oligocene and Quaternary dinoflagellate cysts, ODP Site 1172, East Tasman Plateau [online], *Proc. Ocean Drill. Program Sci. Results*, *189*, 48 pp. (Available at http://www-odp.tamu.edu/publications/189_SR/106/106.htm)

Brinkhuis, H., et al. (2006), Episodic fresh surface waters in the Eocene Arctic Ocean, *Nature*, *441*, 606–609.

Brumsack, H.-J. (2006), Trace metal content of recent organic carbon-rich sediments: Implications for Cretaceous black shale formation, *Palaeogeogr. Palaeoclimatol. Palaeoecol.*, *232*, 344–361.

Bujak, J. P., and H. Brinkhuis (1998), Global warming and dinocyst changes across the Paleocene/Eocene epoch boundary, in *Late Paleocene–Early Eocene Climatic and Biotic Events in the Marine and Terrestrial Records*, edited by M.-P. Aubry et al., pp. 277–295, Columbia Univ. Press, New York.

Bujak, J. P., and D. C. Mudge (1994), A high-resolution North Sea Eocene dinocyst zonation, *J. Geol. Soc. London*, *151*, 449–462.

Cande, S., and D. V. Kent (1995), Revised calibration of the geomagnetic polarity timescale for the Late Cretaceous and Cenozoic, *J. Geophys. Res.*, *111*, 6093–6095.

Colosimo, A. B., T. J. Bralower, and J. C. Zachos (2005), Evidence for lysocline shoaling at the Paleocene/Eocene thermal maximum on Shats-ky Rise, northwest Pacific [online], *Proc. Ocean Drill. Program Sci. Results*, *198*, 36 pp. (Available at http://www-odp.tamu.edu/publications/198_SR/VOLUME/CHAPTERS/112.PDF)

Cramer, B. S., and D. V. Kent (2005), Bolide summer: The Paleocene/Eocene thermal maximum as a response to an extraterrestrial trigger, *Palaeogeogr. Palaeoclimatol. Palaeoecol.*, *224*, 144–166.

Cramer, B. S., J. D. Wright, D. V. Kent, and M.-P. Aubry (2003), Orbital climate forcing of $\delta^{13}C$ excursions in the late Paleocene–early Eocene (chrons C24n–C25n), *Paleoceanography*, *18*(4), 1097, doi:10.1029/2003PA000909.

Crouch, E. M., and H. Brinkhuis (2005), Environmental change across the Paleocene-Eocene transition from eastern New Zealand: A marine palynological approach, *Mar. Micropaleontol.*, *56*, 138–160.

Crouch, E. M., C. Heilmann-Clausen, H. Brinkhuis, H. E. G. Morgans, K. M. Rogers, H. Egger, and B. Schmitz (2001), Global dinoflagellate event associated with the late Paleocene thermal maximum, *Geology*, *29*, 315–318.

Crouch, E. M., H. Brinkhuis, H. Visscher, T. Adatte, and M.-P. Bolle (2003), Late Paleocene–early Eocene dinoflagellate cyst records from the Tethys: Further observations on the global distribution of *Apectodinium*, in *Causes and Consequences of Globally Warm Climates in the Early Paleogene*, edited by S. L. Wing et al., *Spec. Pap. Geol. Soc. Am.*, *369*, 113–131.

Dale, B. (1996), Dinoflagellate cyst ecology: Modeling and geological applications, in *Palynology: Principles and Applications*, edited by J. Jansonius and D. C. McGregor, pp. 1249–1276, Am. Assoc. of Stratigr. Palynol. Found., Dallas, Tex.

Demicco, R. V., and T. K. Lowenstein (2003), Atmospheric pCO_2 since 60 Ma from records of seawater pH, calcium, and primary carbonate mineralogy, *Geology*, 31, 793–796.

de Vernal, A., et al. (2001), Dinoflagellate cyst assemblages as tracers of sea-surface conditions in the northern North Atlantic, Arctic and sub-Arctic seas: The new ''n-677'' data base and its application for quantitative paleoceanographic reconstruction, *J. Quat. Sci.*, 16, 681–698.

de Vernal, A., C. Hillaire-Marcel, W. R. Peltier, and A. J. Weaver (2002), Structure of the upper water column in the northwest North Atlantic: Modern versus Last Glacial Maximum conditions, *Paleoceanography*, 17(4), 1050, doi:10.1029/2001PA000665.

de Vernal, A., et al. (2005), Reconstruction of sea-surface conditions at middle to high latitudes of the Northern Hemisphere during the Last Glacial Maximum (LGM) based on dinoflagellate cyst assemblages, *Quat. Sci. Rev.*, 24, 897–924.

Dickens, G. R. (2000), Methane oxidation during the late Paleocene thermal maximum, *Bull. Soc. Geol. Fr.*, 171, 37–49.

Dickens, G. R. (2001), Carbon addition and removal during the late Palaeocene thermal maximum: Basic theory with a preliminary treatment of the isotope record at Ocean Drilling Program Site 1051, Blake Nose, in *Western North Atlantic Paleogene and Cretaceous Paleoceanography*, edited by D. Kroon et al., *Geol. Soc. Spec. Publ.*, 183, 293–305.

Dickens, G. R., J. R. O'Neil, D. K. Rea, and R. M. Owen (1995), Dissociation of oceanic methane hydrate as a cause of the carbon isotope excursion at the end of the Paleocene, *Paleoceanography*, 10, 965–971.

Dickens, G. R., M. M. Castillo, and J. C. G. Walker (1997), A blast of gas in the latest Paleocene: Simulating first-order effects of massive dissociation of oceanic methane hydrate, *Geology*, 25, 259–262.

Egger, H., J. Fenner, C. Heilmann-Clausen, F. Rögl, R. Sachsenhofer, and B. Schmitz (2003), Paleoproductivity of the northwestern Tethyan margin (Anthering section, Austria) across the Paleocene-Eocene transition, in *Causes and Consequences of Globally Warm Climates in the Early Paleogene*, edited by S. L. Wing et al., *Spec. Pap. Geol. Soc. Am.*, 369, 133–146.

Eldrett, J. S., I. C. Harding, J. V. Firth, and A. P. Roberts (2004), Magnetostratigraphic calibration of Eocene-Oligocene dinoflagellate cyst biostratigraphy from the Norwegian-Greenland Sea, *Mar. Geol.*, 204, 91–127.

Fensome, R. A., and G. L. Williams (2004), *The Lentin and Williams Index of Fossil Dinoflagellates 2004 Edition*, *Contrib. Ser.*, vol. 42, 909 pp., Am. Assoc. of Stratigr. Palynol. Found., College Station, Tex.

Fricke, H. C., and S. L. Wing (2004), Oxygen isotope and paleobotanical estimates of temperature and δ^{18}O-latitude gradients over North America during the early Eocene, *Am. J. Sci.*, 304, 612–635.

Gavrilov, Y., E. A. Shcherbinina, and H. Oberhänsli (2003), Paleocene-Eocene boundary events in the northeastern Peri-Tethys, in *Causes and Con-

sequences of Globally Warm Climates in the Early Paleogene*, edited by S. L. Wing et al., *Spec. Pap. Geol. Soc. Am.*, 369, 147–168.

Greenwood, D. R., and S. L. Wing (1995), Eocene continental climates and latitudinal temperature gradients, *Geology*, 23, 1044–1048.

Hallock, P., I. Premoli Silva, and A. Boersma (1991), Similarities between planktonic and larger foraminiferal evolutionary trends through Paleogene paleoceanographic changes, *Palaeogeogr. Palaeoclimatol. Palaeoecol.*, 83, 49–64.

Haq, B. U., and G. P. Lohmann (1976), Early Cenozoic calcareous nannoplankton biogeography of the Atlantic Ocean, *Mar. Micropaleontol.*, 1, 119–194.

Heilmann-Clausen, C. (1985), Dinoflagellate stratigraphy of the uppermost Danian to Ypresian in the Viborg 1 borehole, central Jylland, Denmark, *Dan. Geol. Unders*, A7, 1–69.

Heilmann-Clausen, C., and H. Egger (2000), The Anthering outcrop (Austria), a key-section for correlation between Tethys and northwestern Europe near the Paleocene/Eocene boundary, in *Early Paleogene Warm Climates and Biosphere Dynamics*, edited by B. Schmitz et al., *Geol. Foeren. Stockholm Foerh.*, 122, 69.

Higgins, J. A., and D. P. Schrag (2006), Beyond methane: Towards a theory for the Paleocene-Eocene thermal maximum, *Earth Planet. Sci. Lett.*, 245, 523–537.

Hollis, C. J. (2006), Radiolarian faunal turnover through the Paleocene-Eocene transition, Mead Stream, New Zealand, *Eclogae Geol. Helv.*, 99, suppl. 1, S79–S99.

Hopmans, E. C., S. Schouten, R. D. Pancost, M. T. J. van der Meer, and J. S. Sinninghe Damsté (2000), Analysis of intact tetraether lipids in archaeal cell material and sediments by high performance liquid chromatography/atmospheric pressure chemical ionization mass spectrometry, *Rapid Commun. Mass Spectrom.*, 14, 585–589.

Hopmans, E. C., J. W. H. Weijers, E. Schefuß, L. Herfort, J. S. Sinninghe Damsté, and S. Schouten (2004), A novel proxy for terrestrial organic matter in sediments based on branched and isoprenoid tetraether lipids, *Earth Planet. Sci. Lett.*, 224, 107–116.

Huber, M., and D. Nof (2006), The ocean circulation in the Southern Hemisphere and its climatic impacts in the Eocene, *Palaeogeogr. Palaeoclimatol. Palaeoecol.*, 231, 9–28.

Huber, M., and L. C. Sloan (2001), Heat transport, deep waters, and thermal gradients: Coupled simulation of an Eocene greenhouse climate, *Geophys. Res. Lett.*, 28, 3481–3484.

Huber, M., L. C. Sloan, and C. J. Shellito (2003), Early Paleogene oceans and climate: A fully coupled modeling approach using the NCAR CCSM, in *Causes and Consequences of Globally Warm Climates in the Early Paleogene*, edited by S. L. Wing et al., *Spec. Pap. Geol. Soc. Am.*, 369, 25–47.

Huber, M., H. Brinkhuis, C. E. Stickley, K. Döös, A. Sluijs, J. Warnaar, S. A. Schellenberg, and G. L. Williams (2004), Eocene circulation of the Southern Ocean: Was Antarctica kept warm by subtropical waters?, *Paleoceanography*, 19, PA4026, doi:10.1029/2004PA001014.

Huckriede, H., and D. Meischner (1996), Origin and environment of manganese-rich sediments within black-shale basins, *Geochim. Cosmochim. Acta*, 60, 1399–1413.

Jaccard, S. L., G. H. Haug, D. M. Sigman, T. F. Pedersen, H. R. Thierstein, and U. Röhl (2005), Glacial/interglacial changes in subarctic North Pacific stratification, *Science*, 308, 1003–1006.

Jokat, W., G. Uenzelmann-Neben, Y. Kristoffersen, and T. M. Rasmussen (1992), Lomonosov Ridge—A double-sided continental margin, *Geology*, 20, 887–890.

Jokat, W., G. Uenzelmann-Neben, Y. Kristoffersen, and T. M. Rasmussen (1995), New insights into the evolution of the Lomonosov Ridge and the Eurasian Basin, *Geophys. J. Int.*, 120, 378–392.

Kelly, D. C., T. J. Bralower, J. C. Zachos, I. Premoli Silva, and E. Thomas (1996), Rapid diversification of planktonic foraminifera in the tropical Pacific (ODP Site 865) during the late Paleocene thermal maximum, *Geology*, 24, 423–426.

Kennett, J. P., and L. D. Stott (1991), Abrupt deep-sea warming, palaeoceanographic changes and benthic extinctions at the end of the Palaeocene, *Nature*, 353, 225–229.

Koch, P. L., J. C. Zachos, and P. D. Gingerich (1992), Correlation between isotope records in marine and continental carbon reservoirs near the Palaeocene/Eocene boundary, *Nature*, 358, 319–322.

Koch, P. L., J. C. Zachos, and D. L. Dettman (1995), Stable isotope stratigraphy and paleoclimatology of the Paleogene Bighorn Basin (Wyoming, USA), *Palaeogeogr. Palaeoclimatol. Palaeoecol.*, 115, 61–89.

Koopmans, M. P., J. Koster, H. M. E. Van Kaam-Peters, F. Kenig, S. Schouten, W. A. Hartgers, J. W. de Leeuw, and J. S. Sinninghe Damsté (1996), Diagenetic and catagenetic products of isorenieratene: Molecular indicators for photic zone anoxia, *Geochim. Cosmochim. Acta*, 60, 4467–4496.

Laskar, J. (1999), The limits of Earth orbital calculations for geological time-scale use, *Philos. Trans. R. Soc. London, Ser. A*, 357, 1735–1759.

Lourens, L. J., A. Sluijs, D. Kroon, J. C. Zachos, E. Thomas, U. Röhl, J. Bowles, and I. Raffi (2005), Astronomical pacing of late Palaeocene to early Eocene global warming events, *Nature*, 435, 1083–1087.

Lowenstein, T. K., and R. V. Demicco (2006), Elevated Eocene atmospheric CO_2 and its subsequent decline, *Science*, 313, 1928.

Luterbacher, H. P., et al. (2004), The Paleogene period, in *A Geologic Time Scale 2004*, edited by F. M. Gradstein et al., pp. 384–408, Cambridge Univ. Press, Cambridge, U. K.

Markwick, P. J. (1998), Fossil crocodilians as indicators of Late Cretaceous and Cenozoic climates: Implications for using palaeontological data in reconstructing palaeoclimate, *Palaeogeogr. Palaeoclimatol. Palaeoecol.*, 137, 205–271.

Marret, F., and K. A. F. Zonneveld (2003), Atlas of modern organic-walled dinoflagellate cyst distribution, *Rev. Palaeobot. Palynol.*, 125, 1–200.

Moran, K., et al. (2006), The Cenozoic palaeoenvironment of the Arctic Ocean, *Nature*, 441, 601–605.

Ogg, J. G., and A. G. Smith (2004), The geomagnetic polarity time scale, in *A Geologic Time Scale 2004*, edited by F. M. Gradstein et al., Cambridge Univ. Press, Cambridge, U. K.

Pagani, M., J. C. Zachos, K. H. Freeman, B. Tipple, and S. Bohaty (2005), Marked decline in atmospheric carbon dioxide concentrations during the Paleogene, *Science*, 309, 600–603.

Pagani, M., K. Caldeira, D. Archer, and J. C. Zachos (2006a), An ancient carbon mystery, *Science*, 314, 1556–1557.

Pagani, M., N. Pedentchouk, M. Huber, A. Sluijs, S. Schouten, H. Brinkhuis, J. S. Sinninghe Damsté, G. R. Dickens, and Expedition-Scientists

(2006b), Arctic hydrology during global warming at the Palaeocene-Eocene thermal maximum, *Nature*, 442, 671–675.

Paillard, D., L. Labeyrie, and P. Yiou (1996), Macintosh Program Performs time-Series Analysis, *Eos Trans. AGU*, 77(39), 379.

Pälike, H., N. J. Shackleton, and U. Röhl (2001), Astronomical forcing in late Eocene marine sediments, *Earth Planet. Sci. Lett.*, 193, 589–602.

Pälike, H., D. J. A. Spofforth, M. O'Regan, and J. Gattacceca (2008), Orbital scale variations and timescales from the Arctic Ocean, *Paleoceanography*, doi:10.1029/2007PA001490, in press.

Pearson, P. N., and M. R. Palmer (2000), Atmospheric carbon dioxide concentrations over the past 60 million years, *Nature*, 406, 695–699.

Pearson, P. N., B. E. van Dongen, C. J. Nicholas, R. D. Pancost, S. Schouten, J. M. Singano, and B. S. Wade (2007), Stable warm tropical climate through the Eocene Epoch, *Geology*, 35, 211–214.

Powell, A. J., H. Brinkhuis, and J. P. Bujak (1996), Upper Paleocene - Lower Eocene dinoflagellate cyst sequence biostratigraphy of southeast England, in *Correlation of the Early Paleogene in Northwest Europe*, edited by R. W. O. B. Knox et al., *Geol. Soc. Spec. Publ.*, 101, 145–183.

Pross, J., and H. Brinkhuis (2005), Organic-walled dinoflagellate cysts as paleoenvironmental indicators in the Paleogene; a synopsis of concepts, *Palaeontol. Z.*, 79, 53–59.

Rachold, V., and H.-J. Brumsack (2001), Inorganic geochemistry of Albian sediments from the Lower Saxony basin NW Germany: Palaeoenvironmental constraints and orbital cycles, *Palaeogr. Palaeoclimatol. Palaeoecol.*, 174, 121–143.

Richter, T. O., S. Van der Gast, R. Koster, A. Vaars, R. Gieles, H. C. De Stigter, H. De Haas, and T. C. E. Van Weering (2006), The Avaatech XRF core scanner: Technical description and applications to NE Atlantic sediments, in *New Techniques in Sediments Core Analysis*, edited by R. G. Rothwell, *Geol. Soc., Spec. Publ.*, 267, 39–51.

Rochon, A., A. de Vernal, J. L. Turon, J. Mathiessen, and M. J. Head (1999), *Distribution of Recent Dinoflagellate Cysts in Surface Sediments From the North Atlantic Ocean and Adjacent Seas in Relation to Sea-Surface Parameters*, *Contrib. Ser.*, vol. 35, 150 pp., Am. Assoc. of Stratigr. Palynol. Found., College Station, Tex.

Röhl, U., and L. J. Abrams (2000), High-resolution, downhole and non-destructive core measurements from Sites 999 and 1001 in the Caribbean Sea: Application to the late Paleocene thermal maximum, *Proc. Ocean Drill. Program Sci. Results*, 165, 191–203.

Röhl, U., T. J. Bralower, G. Norris, and G. Wefer (2000), A new chronology for the late Paleocene thermal maximum and its environmental implications, *Geology*, 28, 927–930.

Röhl, U., R. D. Norris, and J. G. Ogg (2003), Cyclostratigraphy of upper Paleocene and lower Eocene sediments at Blake Nose Site 1051(western North Atlantic), in *Causes and Consequences of Globally Warm Climates in the Early Paleogene*, edited by S. L. Wing et al., *Spec. Pap. Geol. Soc. Am.*, 369, 567–589.

Röhl, U., H. Brinkhuis, C. E. Stickley, M. Fuller, S. A. Schellenberg, G. Wefer, and G. L. Williams (2004), Sea level and astronomically induced environmental changes in middle and late Eocene sediments from the East

Tasman Plateau, in *The Cenozoic Southern Ocean: Tectonics, Sedimentation, and Climate Change Between Australia and Antarctica, AGU Geophys. Monogr. Ser.*, vol. 151, edited by N. F. Exon, J. P. Kennett, and M. J. Malone, pp. 127–151, AGU, Washington, D. C.

Röhl, U., T. Westerhold, S. Monechi, E. Thomas, J. C. Zachos, and B. Donner (2005), The third and final early Eocene thermal maximum: Characteristics, timing, and mechanisms of the "X" event, paper presented at Annual Meeting, Geol. Soc. of Am., Boulder, Colo.

Röhl, U., T. Westerhold, T. J. Bralower, and J. C. Zachos (2007), On the duration of the Paleocene-Eocene thermal maximum (PETM), *Geochem. Geophys. Geosyst.*, 8, Q12002, doi:10.1029/2007GC001784.

Schouten, S., E. C. Hopmans, E. Schefuß, and J. S. Sinninghe Damsté (2002), Distributional variations in marine crenarchaeotal membrane lipids: A new tool for reconstructing ancient sea water temperatures?, *Earth Planet. Sci. Lett.*, 204, 265–274.

Schouten, S., C. Huguet, E. C. Hopmans, M. V. M. Kienhuis, and J. S. Sinninghe Damsté (2007a), Analytical methodology for TEX_{86} paleothermometry by high-performance liquid chromatography/atmospheric pressure chemical ionization-mass spectrometry, *Anal. Chem.*, 79, 2940–2944.

Schouten, S., M. Woltering, W. I. C. Rijpstra, A. Sluijs, H. Brinkhuis, and J. S. Sinninghe Damsté (2007b), The Paleocene-Eocene carbon isotope excursion in higher plant organic matter: Differential fractionation of angiosperms and conifers in the Arctic, *Earth Planet. Sci. Lett.*, 258, 581–592.

Shellito, C. J., L. C. Sloan, and M. Huber (2003), Climate model sensitivity to atmospheric CO_2 levels in the early-middle Paleogene, *Palaeogeogr. Palaeoclimatol. Palaeoecol.*, 193, 113–123.

Sinninghe Damsté, J. S., S. G. Wakeham, M. E. Kohnen, J. M. Hayes, and J. W. de Leeuw (1993), A 6,000-year sedimentary molecular record of chemocline excursions in the Black Sea, *Nature*, 362, 827–829.

Sloan, L. C., and D. K. Rea (1996), Atmospheric carbon dioxide and early Eocene climate: A general circulation modeling sensitivity study, *Palaeogeogr. Palaeoclimatol. Palaeoecol.*, 119, 275–292.

Sluijs, A., H. Brinkhuis, C. E. Stickley, J. Warnaar, G. L. Williams, and M. Fuller (2003), Dinoflagellate cysts from the Eocene/Oligocene transition in the Southern Ocean: Results from ODP Leg 189 [online], *Proc. Ocean Drill. Program Sci. Results*, F. 189, 1–42. (Available at http://www-odp.tamu.edu/publications/189_SR/104/104.htm)

Sluijs, A., J. Pross, and H. Brinkhuis (2005), From greenhouse to icehouse; organic-walled dinoflagellate cysts as paleoenvironmental indicators in the Paleogene, *Earth Sci. Rev.*, 68, 281–315.

Sluijs, A., et al. (2006), Subtropical Arctic Ocean temperatures during the Palaeocene/Eocene thermal maximum, *Nature*, 441, 610–613.

Sluijs, A., H. Brinkhuis, S. Schouten, S. M. Bohaty, C. M. John, J. C. Zachos, J. S. Sinninghe Damsté, E. M. Crouch, and G. R. Dickens (2007a), Environmental precursors to light carbon input at the Paleocene/Eocene boundary, *Nature*, 450, 1218–1221.

Sluijs, A., G. J. Bowen, H. Brinkhuis, L. J. Lourens, and E. Thomas (2007b), The Palaeocene-Eocene thermal maximum super greenhouse: Biotic and

geochemical signatures, age models and mechanisms of global change, in *Deep Time Perspectives on Climate Change: Marrying the Signal From Computer Models and Biological Proxies, TMS Spec. Publ.*, vol. 2, edited by M. Williams et al., pp. 323–349, Geol. Soc., London.

Smith, T., K. D. Rose, and P. D. Gingerich (2006), Rapid Asia–Europe–North America geographic dispersal of earliest Eocene primate *Teilhardina* during the Paleocene–Eocene thermal maximum, *Proc. Natl. Acad. Sci. U. S. A.*, 103, 11,223–11,227.

Stein, R. (2007), Upper Cretaceous/lower Tertiary black shales near the North Pole: Organic-carbon origin and source-rock potential, *Mar. Pet. Geol.*, 24, 67–73.

Stein, R., B. Boucsein, and H. Meyer (2006), Anoxia and high primary production in the Paleogene central Arctic Ocean: First detailed records from Lomonosov Ridge, *Geophys. Res. Lett.*, 33, L18606, doi:10.1029/2006GL026776.

Steurbaut, E., R. Magioncalda, C. Dupuis, S. Van Simaeys, E. Roche, and M. Roche (2003), Palynology, paleoenvironments, and organic carbon isotope evolution in lagoonal Paleocene-Eocene boundary settings in north Belgium, in *Causes and Consequences of Globally Warm Climates in the Early Paleogene*, edited by S. L. Wing et al., *Spec. Pap. Geol. Soc. Am.*, 369, 291–317.

Stickley, C. E., H. Brinkhuis, S. A. Schellenberg, A. Sluijs, U. Röhl, M. Fuller, M. Grauert, M. Huber, J. Warnaar, and G. L. Williams (2004), Timing and nature of the deepening of the Tasmanian Gateway, *Paleoceanography*, 19, PA4027, doi:10.1029/2004PA001022.

Stockmarr, J. (1972), Tablets with spores used in absolute pollen analysis, *Pollen Spores*, 13, 615–621.

Thomas, D. J., J. C. Zachos, T. J. Bralower, E. Thomas, and S. Bohaty (2002), Warming the fuel for the fire: Evidence for the thermal dissociation of methane hydrate during the Paleocene-Eocene thermal maximum, *Geology*, 30, 1067–1070.

Thomas, E. (1989), Development of Cenozoic deep-sea benthic foraminiferal faunas in Antarctic waters, *Geol. Soc. Spec. Publ. London.*, 47, 283–296.

Thomas, E., and N. J. Shackleton (1996), The Palaeocene-Eocene benthic foraminiferal extinction and stable isotope anomalies, in *Correlation of the Early Paleogene in Northwestern Europe*, edited by R. W. O. B. Knox et al., *Geol. Soc. Spec. Publ.*, 101, 401–441.

Tjallingii, R., U. Röhl, M. Kölling, and T. Bickert (2007), Influence of the water content on X-ray fluorescence core-scanning measurements in soft marine sediments, *Geochem. Geophys. Geosyst.*, 8, Q02004, doi:10.1029/2006GC001393.

Tripati, A., and H. Elderfield (2005), Deep-sea temperature and circulation changes at the Paleocene-Eocene thermal maximum, *Science*, 308, 1894–1898.

Tripati, A., J. Zachos, L. Marincovich Jr., and K. Bice (2001), Late Paleocene Arctic coastal climate inferred from molluscan stable and radiogenic isotope ratios, *Palaeogeogr. Palaeoclimatol. Palaeoecol.*, 170, 101–113.

Warnaar, J. (2006), Climatological implications of Australian-Antarctic separation, 144 pp., Ph.D. thesis, Lab. of Palaeobot. and Palynol., Utrecht Univ., Utrecht, Netherlands.

Wedepohl, K. H. (1971), Environmental influence on the chemical composition of shales

and clays, in *Physics and Chemistry of the Earth*, vol. 8, edited by L. H. Ahrens et al., pp. 305–333, Pergamon, Oxford, U. K.

Weijers, J. W. H., S. Schouten, A. Sluijs, H. Brinkhuis, and J. S. Sinninghe Damsté (2007), Warem arctic continents during the Palaeocene-Eocene thermal maximum, *Earth Planet. Sci. Lett.*, *261*, 230–238.

Westerhold, T., U. Röhl, J. Laskar, I. Raffi, J. Bowles, L. J. Lourens, and J. C. Zachos (2007), On the duration of magnetochrons C24r and C25n and the timing of early Eocene global warming events: Implications from the Ocean Drilling Program Leg 208 Walvis Ridge depth transect, *Paleoceanography*, *22*, PA2201, doi:10.1029/2006PA001322.

Wing, S. L., G. J. Harrington, F. A. Smith, J. I. Bloch, D. M. Boyer, and K. H. Freeman (2005), Transient floral change and rapid global warming at the Paleocene-Eocene boundary, *Science*, *310*, 993–996.

Wrenn, J. H., and S. W. Beckmann (1982), Maceral, total organic carbon, and palynological analyses of Ross Ice Shelf Project site J9 cores, *Science*, *216*, 187–189.

Yapp, C. J. (2004), $Fe(CO_3)OH$ in goethite from a mid-latitude North American Oxisol: Estimate of atmospheric CO_2 concentration in the early Eocene "climatic optimum," *Geochim. Cosmochim. Acta*, *68*, 935–947.

Zachos, J. C., K. C. Lohmann, J. C. G. Walker, and S. W. Wise (1993), Abrupt climate change and transient climates during the Palaeogene: A marine perspective, *J. Geol.*, *101*, 191–213.

Zachos, J. C., L. D. Stott, and K. C. Lohmann (1994), Evolution of early Cenozoic marine temperatures, *Paleoceanography*, *9*, 353–387.

Zachos, J., M. Pagani, L. Sloan, E. Thomas, and K. Billups (2001), Trends, rhythms, and aberrations in global climate 65 Ma to present, *Science*, *292*, 686–693.

Zachos, J. C., M. W. Wara, S. Bohaty, M. L. Delaney, M. R. Petrizzo, A. Brill, T. J. Bralower, and I. Premoli Silva (2003), A transient rise in tropical sea surface temperature during the Paleocene-Eocene thermal maximum, *Science*, *302*, 1551–1554.

Zachos, J. C., et al. (2005), Rapid acidification of the ocean during the Paleocene-Eocene thermal maximum, *Science*, *308*, 1611–1615.

Zachos, J. C., S. Schouten, S. Bohaty, T. Quattlebaum, A. Sluijs, H. Brinkhuis, S. Gibbs, and T. J. Bralower (2006), Extreme warming of mid-latitude coastal ocean during the Paleocene-Eocene thermal maximum: Inferences from TEX_{86} and isotope data, *Geology*, *34*, 737–740.

—————————————

H. Brinkhuis, F. Sangiorgi, and A. Sluijs, Palaeoecology, Laboratory of Palaeobotany and Palynology, Institute of Environmental Biology, Utrecht University, Budapestlaan 4, NL-3584 CD Utrecht, Netherlands.

H.-J. Brumsack, Institute for Chemistry and Biology of the Marine Environment (ICBM), University of Oldenburg, P.O. Box 2503, D-26111 Oldenburg, Germany.

U. Röhl, Center for Marine Environmental Sciences (MARUM), Bremen University, Leobener Strasse, D-28359 Bremen, Germany.

S. Schouten, Department of Marine Biogeochemistry and Toxicology, Royal Netherlands Institute for Sea Research (NIOZ), P.O. Box 59, NL-1790 AB, Den Burg, Texel, Netherlands.

J. S. Sinninghe Damsté, Department of Earth Sciences, Utrecht University, Budapestlaan 4, NL-3584 CD Utrecht, Netherlands.